FULL CRITICAL REVIEW

Nanocrystallisation in oxyfluoride systems: mechanisms of crystallisation and photonic properties

A. de Pablos-Martín, A. Durán and M. J. Pascual*

Rare earth (RE) doped oxyfluoride glass ceramics possess interesting optical properties with applications in telecommunications and optoelectronics, such as solid state lasers, optical amplifiers, etc. These materials combine the transparency and mechanical and chemical resistance of aluminosilicate glasses with the low phonon energy and facile incorporation of RE ions in the fluoride crystals. The incorporation of RE ions in the crystalline phases enhances the laser emission intensity, a major property of these materials. Transparency is achieved when crystal size is in the nanometric scale, usually below 40 nm, which avoids light scattering. A strict control of the nucleation and crystal growth processes is therefore necessary which requires a deep knowledge of the crystallisation mechanisms. The great activity and publications in this field in the last decades merit a review providing a comparative study of the different nanoglass ceramic systems, their structural and optical characterisation and their main properties and applications. This is the objective of this review paper which includes 232 references. A general discussion on glass nucleation and crystallisation theories and more relevant crystallisation parameters and characterisation techniques are put forward in the first section of the review, focused on nanocrystallisation processes in oxyfluoride systems. In the second section, the principal RE doped glass ceramics are presented. After a general introduction about the luminescence processes, including up- and down-conversion, the behaviour of RE elements in glasses and crystals are discussed. Glass ceramic compositions have been divided as follows: glass ceramics with a glass composition following Wang and Ohwaki's oxyfluoride glass ceramic,[1] and glass ceramics with different matrix compositions, arranged by crystalline phases. Relevant properties, mainly optical and laser, are described in each system along with the most relevant applications of these materials.

Keywords: Nanocrystallisation, Glass ceramics, Rare earth ions, Luminescence, Up-conversion, Down-conversion

Nanocrystallisation in glasses: crystallisation mechanisms

Nanotechnology and nanomaterials are considered as key technologies for the twenty-first century. Among these materials, nanoglass ceramics are expected to play a major role, since they offer an improvement of certain properties which have been discovered only recently.

In 1933, Tammann[2] established the bases of crystallisation in glasses, with two main stages: nucleation and crystal growth. Both processes depend on the temperature and on the matrix and crystalline nuclei composition.

Instituto de Cerámica y Vidrio (CSIC), C/Kelsen 5, Campus de Cantoblanco, 28049 Madrid, Spain

*Corresponding author, email mpascual@icv.csic.es

The main theoretical studies concerning nucleation and crystallisation of glasses were developed in the sixties by Jackson,[3] Thakur et al.,[4] Turnbull and Cohen,[5] Uhlmann and Chalmers[6] and Hammel.[7] An induction time previous to the nucleation process was suggested,[8] in order to complete the classical nucleation and crystallisation theories.

The variation of the Gibbs energy for nucleation is explained by two different factors: a negative one, corresponding to the crystallisation energy, and a positive factor, which includes the energy barrier necessary for the formation of a new surface. This leads to the definition of a critical radius. Above this radius, the first factor is predominant, the nuclei are stable and crystal growth is possible. Taking into account the temperature dependence of the thermodynamic driving force, the critical radius decreases with decreasing temperature. Therefore, the nucleation rate usually

exhibits a maximum slightly above the glass transformation temperature T_g.

Controlled crystallisation of glasses makes the formation of glass ceramics possible; the process is described in several reviews, the most relevant attributable to Hinz,[9] Lillie,[10] Robredo,[11] Tashiro[12] and McMillan.[13]

Glass ceramics can be synthesised by several methods:

(i) conventional melting and thermal treatment methods. The crystallisation is controlled through the following steps: (1) cooling up to a stabilisation temperature, where nucleation takes place; (2) heating up to the crystallisation temperature, where crystal growth occurs; and (3) cooling to room temperature. Some parameters must be controlled to carry out this process:[14–23] temperature range where the nucleation takes place; temperature for maximum nucleation rate; nucleation and crystallisation rate; activation energy; type of crystallisation, that is, superficial or volumetric; the crystalline fraction and dimensionality of the crystal growth. Nucleation can also take place assisted by nucleanting agents. Addition of such nucleants was introduced by Stookey[24,25] and industrially developed by Corning Glass Works. Phase separation in the parent glasses has a great influence in the subsequent crystallisation,[26] and is directly dependent on undercooling. A phase enriched in network modifiers reduces the diffusion enthalpy and nucleation is facilitated[27]

(ii) sol–gel. A chemical solution (sol) is thermally treated and aged to produce the fine particles in a network (gel). Glass ceramics are obtained on heat treatment of the gel. Moreover, the precursor sol can be deposited on a substrate to form a film, cast into a container with the desired shape, to obtain glasses, fibres and membranes, or used to synthesise powders (microspheres and nanospheres). The main advantages versus the melting method are lower working temperature and higher homogeneity of the glasses. For glass ceramics obtained by this method, three main applications can be highlighted from the literature: (1) dielectric glass ceramics. Li *et al.*[28] developed BPO_4 and $Si_3(PO_4)_4$ glass ceramics, for high frequency multilayer inductors; (2) bioactive glass ceramics. Worth mentioning are the works of Cai *et al.* on development of phosphate glass ceramics,[29] and Chen *et al.* who obtained $Na_2Ca_2Si_3O_9$ and extensive formation of amorphous bone-like apatite;[30] and (3) photonics, based on rare earth (RE) doped materials,[31,32] where the nanosize of the precipitated crystals is crucial on order to avoid light scattering and increase laser emission.

Despite the great technological potential of nanocrystalline glass ceramics, the fundamentals of the crystallisation mechanisms are not fully understood. Theories of crystallisation are usually restricted to isochemical systems in which the crystalline phase has the same chemical composition as the glass matrix. However, the challenge of obtaining large volume concentrations of crystals with sizes in the 5–50 nm range and narrow size distribution can only be achieved in multicomponent systems and by controlling the change in the chemical composition of the glass matrix and the interphase formed during nucleation and crystal growth.

Since the nineties, crystallisation of nanosized crystals has been analysed mainly by two different methods:

(i) crystallisation studies through crystallochemistry and thermodynamic procedures; important work was performed by Stoch[33] and Sroda *et al.*[34] who analysed the crystallisation of different species by DTA and considered the ionicity of the bonds involved

(ii) in order to complement the classical nucleation and crystallisation theories, a second trend takes into account the change of the composition during the crystallisation process, studying the interphase created in highly viscous liquids such as glass melts near the glass transition temperature. Two cases can be distinguished: (1) the viscosity of the liquid at the interphase is smaller than that of the bulk; this leads to an increase in the crystal growth rate due to enhanced diffusion. On the contrary, if (ii) the viscosity increases, the interphase will act as a diffusional barrier and will notably decelerate the crystal growth velocity. Relevant authors who have studied these phenomena are Rüssel, Avramov, Keding, Petrini Fogaca de Almeida, Bocker and Hill *et al.*[35–39] Rüssel[40] suggested a mechanism for the crystallisation of CaF_2 in aluminosilicate glasses, in which the interphase is enriched in glass formers, increasing the viscosity near the crystals. Thus, a diffusional barrier around each crystal is formed, which hinders further crystal growth. This mechanism opened up a new route in the preparation of nanoglass ceramics, since the nanometric size of the crystals can be controlled via the formation of this viscous barrier.

Superficial stresses developed around crystals, the structure of the melt during cooling and the percolation theories are taken into account for the first time in these works. An interesting explanation is that nucleation takes place into a floppy region if the critical nucleus radius is smaller than this region[51] and, specially if the average number of covalent bonds per network former unit $\langle n \rangle$ is below 2·4.[41] In this case, a monomodal crystal size distribution is obtained. If 2·4 $\langle n \rangle$ 3·17, the network is rigid and nucleation first occurs in the small residual floppy regions and thereafter in the rigid part of the network, resulting in a bimodal crystal size distribution. Avramov *et al.*[42] and Tsakiris *et al.*[43] performed Monte Carlo simulations to study the diffusion process. They assumed a particle moving on a two-dimensional square disordered lattice, containing network formers connected by bonds. Two parameters are decisive for the diffusion analysis: the bond removal probability f and the upper limit of a number of network formers bonds m. For each value of m, a critical value of f, f_c exists. Below this value, the diffusion of the particle is inhibited by the large number of network former bonds, and above it the particle moves more easily through the lattice. Diffusion takes place when the first neighbouring atoms have a number of bonds which is less than the m value; in other words, they are in a floppy state.

The abovementioned authors have greatly influenced more detailed approaches merging nucleation theory

and percolation theory. Quite recently, in collaboration with Rüssel,[44] a model describing the crystal growth was developed taking into account the stress energy developed in the vicinity of the growing crystal. The crystallisation starts rapidly in a floppy region; when this region is totally crystallised, further crystallisation propagates inside the rigid region, giving rise to stress development in the periphery of the crystal, which slows the growth rate. As the stress relaxation is too slow in the rigid region, stress energy can be accumulated.

The simulation parameters f, f_c, m and stress relaxation time τ give an idea of the range of glass compositions which can develop nanocrystals, avoiding those compositions which exhibit stress free matrix, in which crystals are not able to remain nanometric.

Characterisation techniques

Various techniques are used for the complete study of glass ceramics.

Dilatometry allows the determination of the glass transition temperature T_g, softening point T_S and lineal expansion coefficient α, and evaluation of their changes with crystalline fraction.

X-ray diffraction (XRD) permits identification of the crystalline phase and crystalline structure following its evolution with time and temperature of heat treatment, and to calculate the crystalline fraction and crystal sizes.

Differential scanning calorimetry (DSC)[45] gives information about the activation energy of the global crystallisation process and is useful to calculate the Avrami coefficient and the dimensionality of crystal growth, thereby helping to establish the crystallisation mechanism. Donald[46] summarises the different crystallisation mechanisms from the values of Avrami parameter, n and m, which represent the dimensionality of crystal growth from which bulk crystallisation and surface crystallisation may be discerned. The methods outlined in this paper are nowadays a starting point for elucidating the crystallisation mechanism from DTA/DSC results.[47]

Different electron microscopies, such as transmission electron microscopy (TEM) and in high resolution mode, scanning electron microscopy, energy filtered transmission electron microscopy and electron energy loss spectroscopy, allow the estimation of the mean crystal size, identification of phase separation[26] and the recording of compositional elemental mappings.

Nuclear magnetic resonance (NMR) spectroscopy is used to study the first coordination sphere of the glass components.[48] For instance, the partial substitution of fluoride ions by oxygen in aluminosilicate glasses and its structural role in oxyfluoride glasses can be studied with this technique, due to the high sensitivity of ^{19}F to its neighbouring atoms and coordination number.[49]

Other techniques used include Fourier transformation infrared spectroscopy, neutron diffraction, Raman spectroscopy and atomic force microscopy.

In terms of the characterisation of optically active materials, a main aspect to study is the distribution of dopant ions between glassy and crystalline phases, since this is decisive in clarifying the emission mechanism and the efficiency dependence on the crystal size and crystalline fraction. Raman,[50] NMR,[51] electron paramagnetic resonance[52,53] and Mössbauer spectroscopies[54] are useful for establishing a relationship between structure and properties of these materials; together with

absorption and linear emission spectroscopies, the environment of RE elements can be analysed. The change of the lattice parameters when the RE ion is incorporated into the crystal structure can be measured by refined XRD patterns.

Optical measurements at low temperature are useful to minimise the effect of phonons produced by lattice vibrations. Absorbance or transmittance measurements permit the identification of the RE electronic levels. Comparing the spectra of glass and glass ceramics, it is possible to detect changes in the RE environment. From absorption spectra, excitation wavelengths are selected to obtain linear emission spectra, which are useful not only for acquiring the complete energy level diagram of the RE ion in the studied matrix, but also to identify changes or displacements in the bands or even the appearance of new bands. Emission spectroscopy allows the calculation of the lifetime of a certain excited level from the luminescence curves. An effective decay constant τ_{eff} can be described through equation (1) as

$$\tau^{eff} = \frac{\int_0^\infty I(t)t\,dt}{\int_0^\infty I(t)\,dt} \qquad (1)$$

where $I(t)$ is the luminescence intensity at time t after the excitation pulse.

Lifetime values are also useful for identifying different environments in a doped glass ceramic sample, according to the phonon energies and decay processes.[55]

In the emission processes, the relationship between the emission intensity I_{em} and the excitation intensity I_{ex} is

$$I_{em} \propto (I_{ex})^n \qquad (2)$$

where n is the number of infrared photons absorbed per visible photon emitted. Therefore, a plot of $\log I_{em}$ versus $\log I_{ex}$ should yield a straight line with slope n.

The Judd–Ofelt formalism[56,57] allows the radiative lifetimes, branching ratios and transition probabilities to be determined and relates them with the environment of the RE ions.[58] From the room temperature absorption spectra, three parameters are obtained: Ω_2, Ω_4 and Ω_6. Ω_2 is related with short range effects of the glass host, with asymmetry in the vicinity of RE ions and with the covalence between the RE ions and the ligand anions. Ω_2 decreases when the host changes from oxide to fluoride. Ω_6 is related to the rigidity of the solid host in which the lanthanide ions are situated. The ratio Ω_4/Ω_6 is defined as the spectroscopic quality parameter. A decrease in Ω_4 implies that the efficiency of the electronic transition is weak.

Glass ceramics for optically active and passive materials

Transparency is the main required characteristic in nanoglass ceramics for low thermal expansion coefficient materials and transparent materials for optical applications.[59–62]

Transparent nanoglass ceramic materials with low thermal expansion coefficient

Many optical devices such as telescopes and optical cavities require a substrate material with extremely low thermal expansion coefficient and a high thermal shock resistance. In 1968, the Schott Company patented Zerodur, a nanocrystalline transparent glass ceramic in the Li_2O–Al_2O_3–SiO_2 system, which possesses a coefficient of

1

2
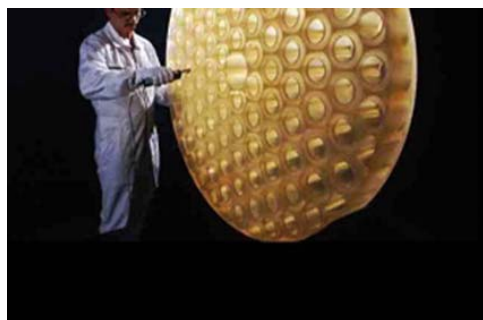
thermal expansion close to zero, suitable for the construction of telescope mirror substrates for astronomy[63–65] (Fig. 1); Clearceram-Z (Ohara) is a similar material. In particular, the space telescopes Hubble and the new James Webb, being developed by NASA, are constructed with these glass ceramics.

Ceran (1973) with high temperature stability and durability, high mechanical stability, low thermal conductivity and thermal shock resistance is extensively applied in cooktop panels, and Robax (1979), an extremely heat resistant transparent glass ceramic, is used in fireplaces and stoves.

In 1969, Beall and Duke[66] described oxide systems based on the crystallisation of spinels, mullite or β-quartz in a vitreous aluminosilicate matrix. The increasing interest in this system is reflected in more recent reports.[67–69]

More recently, Wurth *et al.*[70] have developed nanoglass ceramics from the Robax parent glass, provided by Schott AG, Mainz, Germany. The crystalline phase is a hexagonal high quartz solid solution phase with a nominal composition of $LiAlSi_2O_6$, reaching up to 80 wt-% crystals with retention of transparency (Fig. 2). The sizes of the crystals are in the range 16–22 nm for heat treatments at 750°C from 4 to 120 h. The viscosity of the glass phase increases during the heat treatments, which decelerates crystal growth and eventually prevents further crystallisation. The crystallisation mechanism of $LiAlSi_2O_6$ in this system has been analysed mainly by TEM techniques[71] and is explained as follows. Homogeneous precipitation of nanocrystalline $ZrTiO_4$,[72] which acts as nucleating agent, is accompanied by the formation of an aluminium enriched shell around the $ZrTiO_4$ precipitates, similar to the growth mechanism of CaF_2 nanocrystals, which are surrounded by network former oxides.[44] This Al_2O_3 layer at the $ZrTiO_4$–glass interphase decreases the interphase energy, allowing optimum preconditions for nucleation of the secondary phase, $LiAlSi_2O_6$, and retention of its nanometric crystal size. Nuclei formation in lithium–aluminosilicate glass ceramics was previously reported by Sprengard *et al.*,[73] where TiO_2 is segregated from the glass network, acting as a nucleating agent.

Transparent nanoglass ceramic materials for optically active materials

Nowadays, an interesting and important field of research is focused on the development of optical devices based on materials doped with RE ions for their use in telecommunication systems. In particular, doped phosphate glasses are widely used as host matrices. However, current efforts dedicated to increasing the efficiency of the devices are focused on finding materials with low phonon energy, in order to reduce the multiphonon non-radiative de-excitation and to improve the cross-sections of the rare earth ions; fluoride and chalcogenide based matrices are the most common choices (Table 1).[74–76] However, these glasses present difficult melting and forming characteristics, as well as poor chemical durability and mechanical stability.

The development of oxyfluoride glass ceramics offers a better alternative, because of their low phonon energy, optical transparency and RE ion solubility typical of fluoride matrices, allied to the good mechanical, thermal and chemical properties of oxide glasses.

The most relevant publications within this topic are focused on glass ceramics with different crystalline fluoride phases.

LaF_3

LaF_3 has been extensively studied in oxyfluoride glass ceramics. It has the second lowest phonon energy of the commonly used RE doped matrices (Table 1) and presents a hexagonal crystalline structure.[77] Moreover, a small crystallographic mismatch exists between LaF_3 crystals and REF_3 crystals.

Stoch[33] explained the LaF_3 crystallisation on the basis of the cation–cation interaction. The ionicity of Na–O bonds is much higher than that of La–O; thus, the $[AlO_4]$ tetrahedra tend to bond with Na^+ for compensating their electrical charge, instead of forming bonds with La^{3+}. However, the existence of Al–O–La bonds allows the segregation and crystallisation of LaF_3 from the glass structure.

Crystallisation in glasses within the system Na_2O–Al_2O_3–SiO_2–LaF_3 as determined by DTA has been

Table 1 Table of selected lattice phonon energies of commonly used matrices for Ln^{3+} doping[71–73]

Material	Highest phonon energy/cm^{-1}
Phosphate glass	1200
Silica glass	1100
Fluoride glass	550
Chalcogenide glass	400
LaPO$_4$	1050
YAG	860
YVO$_4$	600
LaF$_3$	300
LaCl$_3$	240
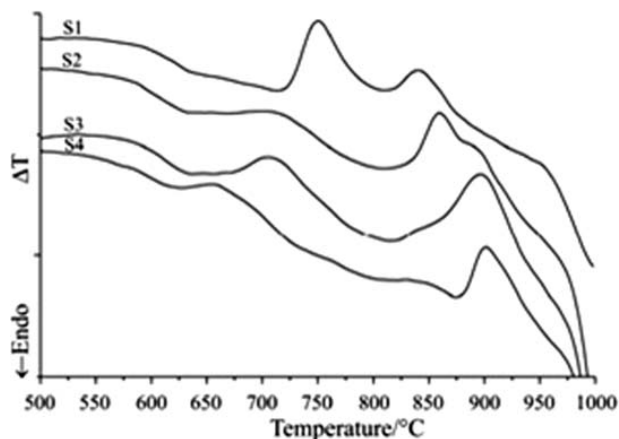
3

discussed in detail.[34] The glass compositions are (51–60) SiO_2–(21–26)Al_2O_3–(16–22)Na_2O–(1–4)LaF_3(mol-%). The crystallisation process was identified through exothermic peaks above T_g (Fig. 3). The propension for crystallisation of these glasses was studied from the crystallisation temperatures T_{cryst}, crystallisation enthalpy ΔH_{cryst} and thermal stability parameter $\Delta T = T_{cryst} - T_g$. Heat treatments at the maximum crystallisation temperature of LaF_3 were carried out, and the structure and size of the precipitated crystals were studied by XRD and TEM. The crystallisation mechanism of LaF_3 was explained through crystallochemical arguments.

  (i) silica: increasing silica content increases the viscosity. High silica contents with a fixed ratio $La_2F_6/2(Al_2O_3 + Na_2O)$ produce an increase in T_g and a reduction of heat capacity, ΔC_p, making evident the increase in the glass network strength. In addition, the temperature of the DTA crystallisation peak shifts to higher values, the crystallisation enthalpy ΔH_{cer} decreases and the thermal stability index $\Delta T = T_{cryst} - T_g$ increases, showing the lower propension for crystallisation of the glass

  (ii) alumina: a reduction in alumina content makes LaF_3 crystallisation more difficult, except if this reduction is accompanied by increasing amounts of Na_2O and LaF_3

  (iii) sodium oxide: the Na_2O/Al_2O_3 ratio defines the degree of saturation of [AlO_4] tetrahedra in the glass network by the Na^+ ions. When the content of modifier ions is too low, lanthanum is retained by aluminium and LaF_3 crystallisation is inhibited

  (iv) lanthanum fluoride: lanthanum compensates the electrical charge of the [AlO_4] and [SiO_4] tetrahedra only in oxygen bonds which are not saturated by Na^+. Thus, the $Na_2O/(SiO_2 + Al_2O_3)$ ratio gives an idea of the ability of LaF_3 crystallisation.

Similar studies were presented in further papers of Sroda et al.[78,79] in which infrared spectroscopy crystallisation analysis is mainly discussed. The studied compositions are (42–56)SiO_2–(24–33)Al_2O_3–(16–21)Na_2O–3LaF_3 (mol-%). Nanoglass ceramics were obtained after heat treatments of 20 min at the corresponding crystallisation peaks with LaF_3 crystallising in the range 625–800°C. This work makes a distinction between first crystallisation state, where LaF_3 crystallisation occurs at temperatures lower than the maximum crystallisation peak, and second crystallisation state, where other species like silicates crystallise at higher temperatures. Characterisation by atomic force microscopy was also carried out. Figure 4 shows the fracture surface of the obtained glass ceramics with crystals appearing after 20 min of treatment at 750°C.

Reben et al.[80] performed the structural characterisation by infrared spectroscopy, following the course of LaF_3 crystallisation and studying the influence of fluoride content and of different fluorine sources in this process. Additional absorption bands in the glass ceramic respect to the parent glass are observed at 350, 270, 255, 206, 166, 130 and 100 cm^{-1}, in agreement with the infrared absorption spectra of LaF_3.

Hémono et al.[81] worked on LaF_3 nanocrystallisation in glasses of composition 40SiO_2–30Al_2O_3–18Na_2O–12LaF_3 and 55SiO_2–20Al_2O_3–15Na_2O–10LaF_3 (mol-%). In Ref. 82, the former glass was studied by TEM, energy filtered transmission electron microscopy and electron energy loss spectroscopy. Figure 5a shows the elemental distribution map of Si in the parent glass. Phase separated regions appear much brighter than the matrix, indicating the presence of Si in phase separated droplets along with La; thus, La and Si appear cosegregated
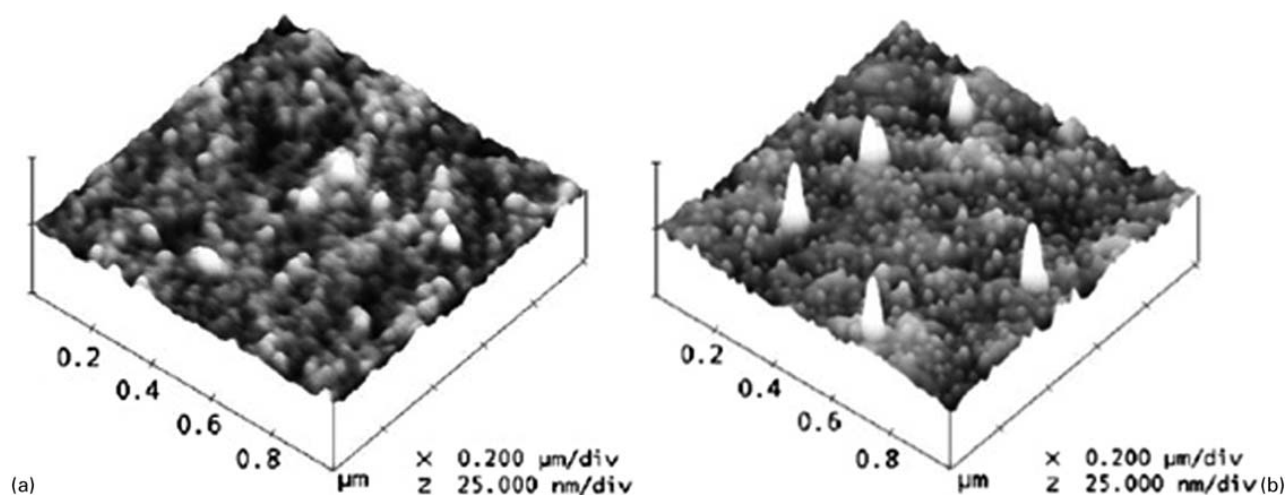
4
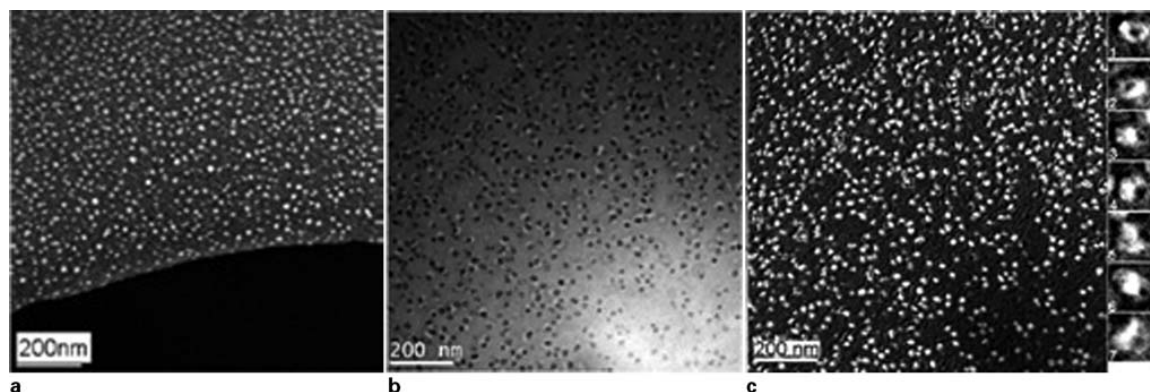
5

within the phase separated droplets. Figure 5*b* shows the Si elemental distribution in the glass ceramic. Nanocrystals appear bright and around 2–5 nm larger than the corresponding bright field image. Several magnified images of nanocrystalline precipitates are also shown in Fig. 5*c*, where small dark regions within bright features are identified, confirming the crystallasation of a La rich phase, corresponding to LaF_3 crystals from the La/Si phase separation nuclei present in the glass. SiO_2 enriched environments form around the crystals, hence inhibiting further crystal growth (Fig. 6).

This mechanism suggested by Hémono *et al.* differs from that of Rüssel in CaF_2 containing system,[44] where phase separation was not detected in the parent glass. Both mechanisms, however, exhibit silica enrichment around the crystals, with the interphase depleted in alumina.

Important contributions to the fluoride crystallisation study have been made with NMR experiments. Muñoz *et al.*[83] confirmed the phase separation zones in the glasses studied in Ref. 81 through ^{19}F NMR. Fluorine in the glasses appears to be involved in Al–F–Na and La–F bonds, the latter being precursors of LaF_3 nucleation, as discussed in Ref. 82. Thermal treatment of the parent glasses induces the diffusion of fluorine from the glass matrix (Al–F–Na bonds) into the La–F bond enriched nuclei, giving rise to a decrease in the concentration of Al–F–Na and an increase in the number of La–F bonds. [SiO_4] structural units must rearrange in order to facilitate crystal growth and, once a silica enriched

region around the crystals is formed, further fluorine diffusion and crystal growth are hindered.
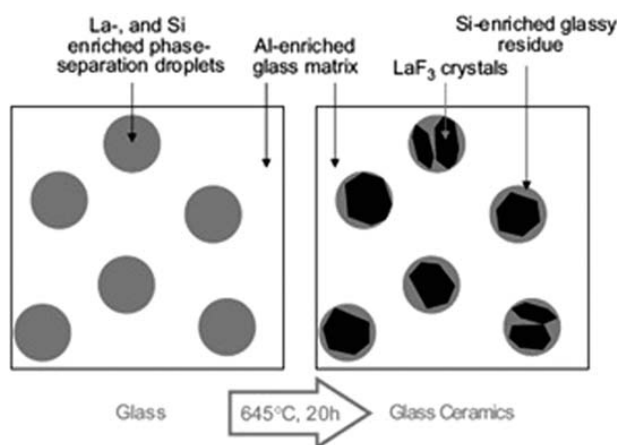
Crystallisation of LaF_3 in the system SiO_2–Al_2O_3–Na_2O–BaO–LaF_3 has also been studied by Youngman and Dejneka[84] through NMR, demonstrating that fluoride content in the crystalline phase depends on the amount of SiO_2 and on the modifier oxide, in this work, Na_2O or BaO. Analysis of the obtained spectra indicates that the intensity of the La–F signal in crystalline environments in glass ceramics increases with the silica content. Two different signals can be distinguished in the studied glasses: one at -185 ppm, attributed to Al–F bonds, and another at -135 ppm, due to Si–F bonds. The first signal increases in the glass ceramics containing Na_2O, while the second does so in those with BaO. Signals corresponding to glassy environments decrease in intensity during the progress of crystallisation. Quantitative analysis shows that in Na_2O containing glass ceramics, the amount of fluoride in LaF_3 crystals grows faster than those with BaO, independent of silica content.

Other important reports about the fluorine sites in oxyfluoride glasses and glass ceramics dependent on the composition have been reported by Kiczenski *et al.*[85] and Stebbins *et al.*[86]
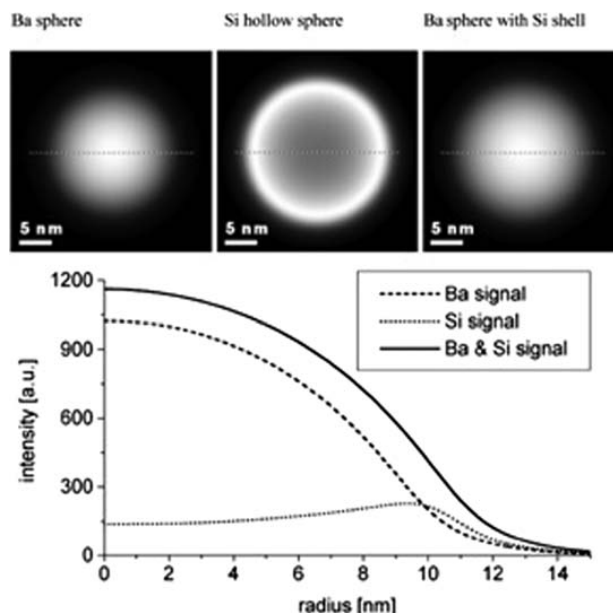
Other fluoride crystalline phases

Rüssel[44] studied the crystallisation of CaF_2 in oxyfluoride glasses following with other fluoride phases. Ritter *et al.*[87] reported photo-thermal-refractive glasses in the Na_2O–K_2O–CaO–CaF_2–Al_2O_3–SiO_2 system. Glasses are irradiated by ultraviolet light, and the nanocrystallisation of CaF_2 takes place only in those irradiated zones.

Bocker *et al.*[88,89] studied the crystallisation of BaF_2 in glass of composition (mol-%): $(100-x)(2Na_2O$–$16K_2O$–$8Al_2O_3$–$74SiO_2)$–$xBaF_2$ ($x=0$–6), which also leads to an increase in the viscosity near the crystals, forming a silica enriched diffusional barrier.[41,79] From this composition, Bhattacharyya *et al.*[90] studied the mechanism by advanced analytical TEM techniques, including simulations, in which the formation of a 1 nm wide SiO_2 shell around the crystals is confirmed (Fig. 7). Analogous to CaF_2 crystallisation,[44] the parent glass of this system does not present phase separation zones. However, ^{19}F NMR characterisation of the parent glass with 6 mol-%BaF_2 gives related structural information.[91] A very small and broad resonance band is detected within the range from -25 to 50 ppm, which can be attributed

6

6   **International Materials Reviews**   2011   VOL 000   NO 000

International Materials Reviews   imr175.3d   30/6/11 01:31:47
The Charlesworth Group, Wakefield +44(0)1924 369598 - Rev 7.51n/W (Jan 20 2003)

7

8

to fluorine in Ba–F clusters within an amorphous environment, similar to the results reported by Muñoz *et al.*[83] in LaF$_3$ containing glasses. A crystal growth model for the composition studied by Bocker and Rüssel,[88] was performed through Monte Carlo simulation.[44] The model fits well the experimental data in a fast increase in initial size without stress development, with a further slowdown of crystal growth, depending on the relaxation time.

Bocker *et al.*[92] analysed the effect of viscosity increases in the crystal–glass interphase due to the depletion of barium and fluorine during the course of crystallisation, which decelerates the corresponding diffusion of atoms forming crystals. By combining the second Fickian law with the fluorine concentration profile (Fig. 8), the diffusion coefficient of fluoride in this matrix at a certain temperature is calculated as $4\cdot5\times10^{-15}\pm1\cdot1\times10^{-15}$ m^2 s^{-1} at 580°C. Bocker *et al.*[93] reported for the first time the formation of a high pressure phase, orthorhombic BaF$_2$, due to the effect of compressive stresses. The formation of a viscous layer around the crystals hinders stress relaxation, leading to the orthorhombic high pressure modification of BaF$_2$.

The interest in tetrafluorides increased after NaYF$_4$ was found to be one of the most efficient near infrared (NIR) to visible up-conversion host materials, since its structure offers different sites to incorporate doping ions, and shows phonon energy of 360 cm^{-1}. Liu *et al.*[94] studied the nanocrystallisation of this phase in an aluminosilicate glass, and analysed the effects of Nd^{3+} addition in its crystallisation. A similar study was reported by Sroda,[95] in the crystallization process of NaLaF$_4$, affected by Er^{3+} ions. de Pablos-Martín *et al.*[96] described the crystallisation mechanism of NaLaF$_4$ and the formation of a diffusional barrier, similar to those work reported in Refs. 44, 82 and 90. Enrichment in SiO$_2$ is evident from TEM techniques. On performing an EELS line scan across a nanocrystal of around 20 nm, a silica concentration profile is developed, showing a shell-like silica distribution (Fig. 9). Muñoz *et al.*[83] described the crystallisation mechanism through ^{19}F NMR measurements (Fig. 10). The
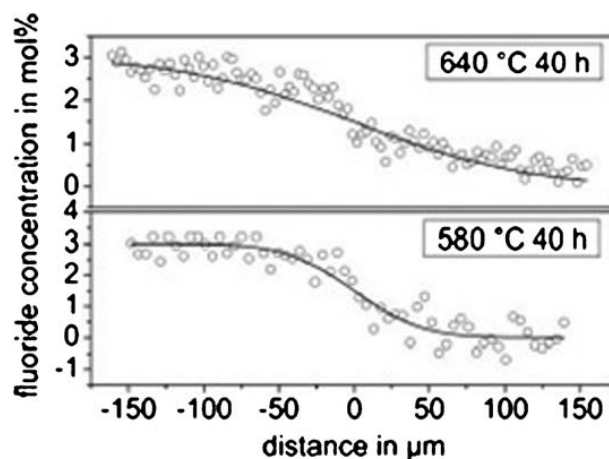
spectrum of the parent glass shows a weak and broad resonance at -180 ppm, assigned to fluorine in Al–F–Na groups, and a larger one centred on -46 ppm, which spreads over the ^{19}F chemical shift range of Na–La–F bonds, indicating the phase separated regions, which give rise to nanocrystals after heat treatment. For long treatment times, NaLaF$_4$ formation is followed by NaF precipitation, which can be explained taking into account the silica shell formed around the crystals. Fluorine diffusion from Al–F–Na groups into NaLaF$_4$ crystals occurs only up to a certain treatment time; thereafter fluorine cannot diffuse anymore to form NaLaF$_4$ crystals and NaF precipitates.
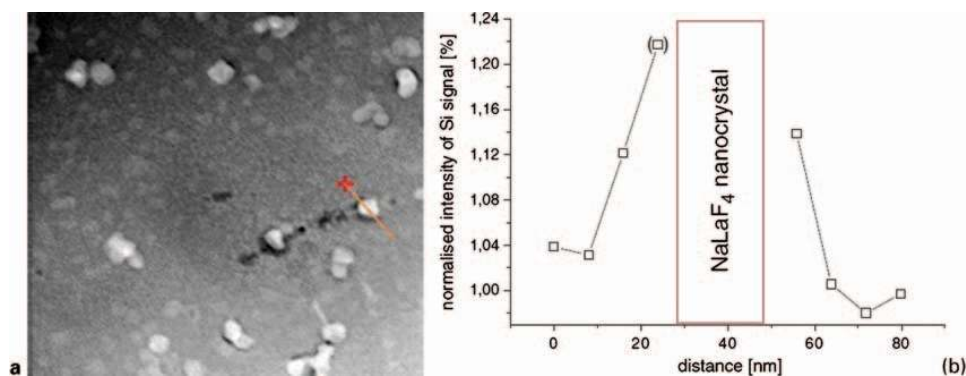
Several questions concerning the fluoride crystallisation mechanism in aluminosilicate systems are still open, even though the topic has been extensively studied in the last 10 years. Fluoride matrices are the key for photonic applications; thus, knowledge of their crystallisation mechanisms, ability of crystallisation and thermodynamic parameters depending on glass composition must be fully understood.

To build a general vision of the analysed crystallisation mechanisms of optically passive and active glass ceramics, we return to the two trends of the crystallisation study. The basis of Stoch and Sroda *et al.* should be used from the very beginning of the study, since this trend is based on theoretical aspects, such as crystallisation enthalpies, bond ionicities, heat capacities and thermal stability indices. Undoubtedly, this study allows the crystallisation mechanism to be predicted. However, a deeper knowledge of the structure and composition of the intherphases formed between glass matrix and crystal, and their evolution during crystallisation as suggested by Rüssel *et al.*, is necessary. Both approaches represent the basis of a better understanding of crystallisation phenomena in non-isochemical systems in general. They foster the future development of glass ceramics hosting functional nanocrystalline precipitates.

RE elements as doping agents in fluoride containing nanoglass ceramics

RE elements have been widely used to activate luminescent and photonic materials based on the properties of their f-shell electrons. Liu and Jacquier[97] have revised the progress in this field, including the

International Materials Reviews imr175.3d 30/6/11 01:31:51
The Charlesworth Group, Wakefield +44(0)1924 369598 - Rev 7.51n/W (Jan 20 2003)

International Materials Reviews 2011 VOL 000 NO 000 7

COLOUR FIGURE

9

principles required to develop and characterise optical materials.

Transparent glass ceramics can be used as active optical devices when they possess the appropriate characteristics for hosting lanthanide ions, thereby allowing the desired optical emissions. In general, a crystal-like environment leads to higher cross-sections, important in the fabrication of more compact devices. Lanthanide ions tend to substitute the cations in the crystalline phase, instead of remaining in the glass matrix.[98] Thus, the optical and mechanical properties of these glass ceramics are the result of combining the features of the glass matrix and the crystalline phases.

The crystalline phase must fulfil certain criteria: (1) to have low phonon energy in order to avoid non-radiative relaxation channels due to excited state energy transfers by phonons, thereby reaching longer lifetimes and higher luminescence efficiencies (Table 1); (2) to be a good host for RE elements, e.g. La^{3+} radius is similar to those of lanthanides, facilitating its substitution in the LaF_3 lattice; and (3) to be thermally stable.

The luminescence properties of doped glass ceramics are related to the microstructure developed during crystallisation, wherein the absorption and scattering are two important phenomena. Location of doping agents into the crystals enhances the radiative decay processes. Some important factors to take into account when using REs as dopants are the lifetime of their excited states and the non-radiative decay channels, which depend on the environment and on their excitation energies.

The doping agent must exhibit certain characteristics, such as emission bands at interesting wavelengths for applications, excitation with an available and affordable source, and having one or more metastable electronic levels.

To confirm the inclusion of the dopant ions into the crystals, certain RE ions are used as structural probes. This is the case of Eu^{3+}, which is widely studied not only in glassy[99–101] and crystalline[102,103] matrices, but also in glass ceramics.[104] The $^5D_0 \rightarrow {}^7F_2$ transition is electrical dipole allowed and sensitive to the local environment, while the $^5D_0 \rightarrow {}^7F_1$ transition is magnetic dipole allowed, and independent of the host matrix. The fluorescence intensity ratio R of $^5D_0 \rightarrow {}^7F_2$ to $^5D_0 \rightarrow {}^7F_1$ transitions is used to establish the degree of both
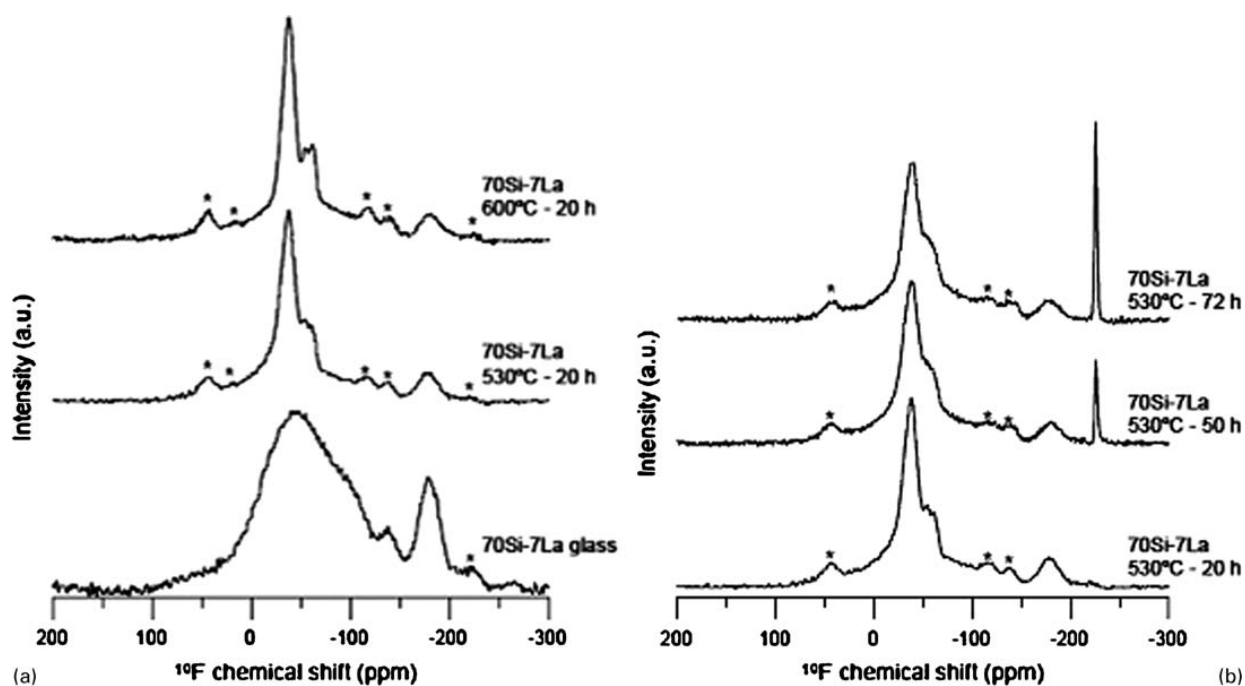
10
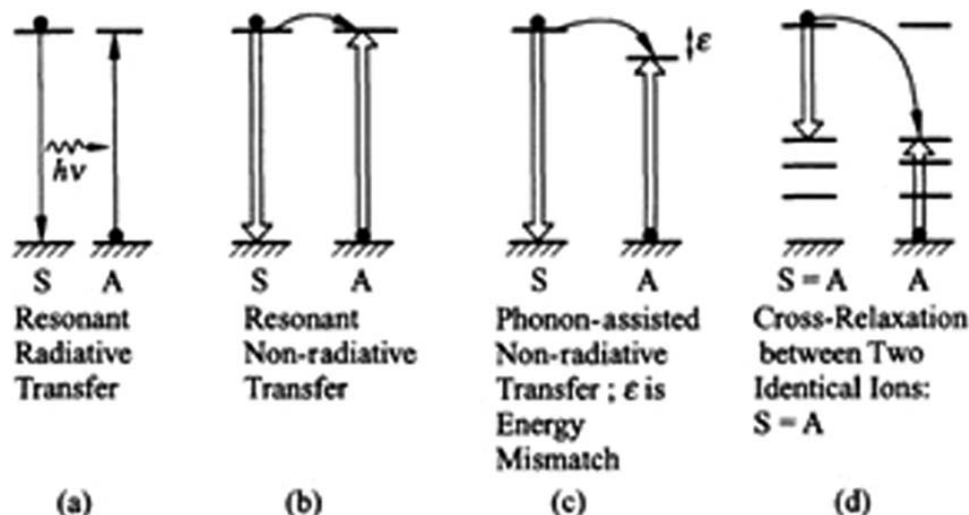
11

asymmetry in the vicinity of Eu^{3+} ions and Eu–O covalence.[105] The emission intensity of the $^5D_0 \rightarrow ^7F_2$ electrical dipole transition is more intense in non-symmetric sites. R also depends on the Judd–Ofelt parameter Ω_2, which is used to describe the short range effects. The higher the value of R, the lower the symmetry of Eu^{3+} ions and more covalent the Eu–O bond.[106,107]

## Up- and down-conversion processes

Up-conversion process

Up-conversion (UC) emission is an anti-Stokes process, in which low excitation photons produce photons of higher energy.[108] Auzel[109] reviewed the UC processes taking place in doped systems through different types of energy transfer between pairs of ions: radiative, non-radiative, resonant and phonon assisted transfer. For a radiative energy transfer (Fig. 11a), photons are emitted by the sensitiser ions S and are then absorbed by the activator ions A within a photon travel distance.

The factors to be controlled in energy transfer processes leading to UC emission include: (1) a phonon energy of the host matrix which is low enough to allow radiative decays; (2) the RE ion concentration, since an increase of the dopant ion concentration reduces the distances between ions and the energy transfer probability is enhanced;[110] (3) temperature, since low temperatures (10–70 K) minimise the network vibrations, and thus the non-radiative decay processes.

UC occurs through a photon avalanche (PA) mechanism. PA was discovered in Pr^{3+} based infrared quantum counters by Chivian et al.[111] Joubert made a complete description of the theoretical treatment of PA process.[112,113] There are two main characteristics of PA: (1) the pump wavelength is only resonant between a metastable state and a higher energy level; in other words, the energy of the excited state exceeds that of the pump photon; and (2) below a power threshold the up-converted fluorescence intensity is weak; above it, the fluorescence increases by orders of magnitude and
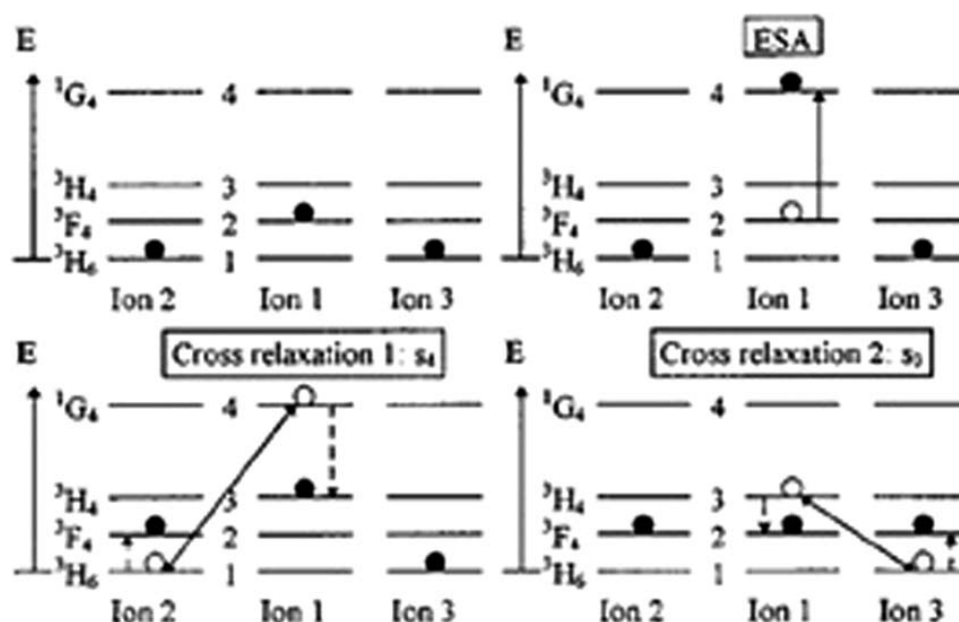
12
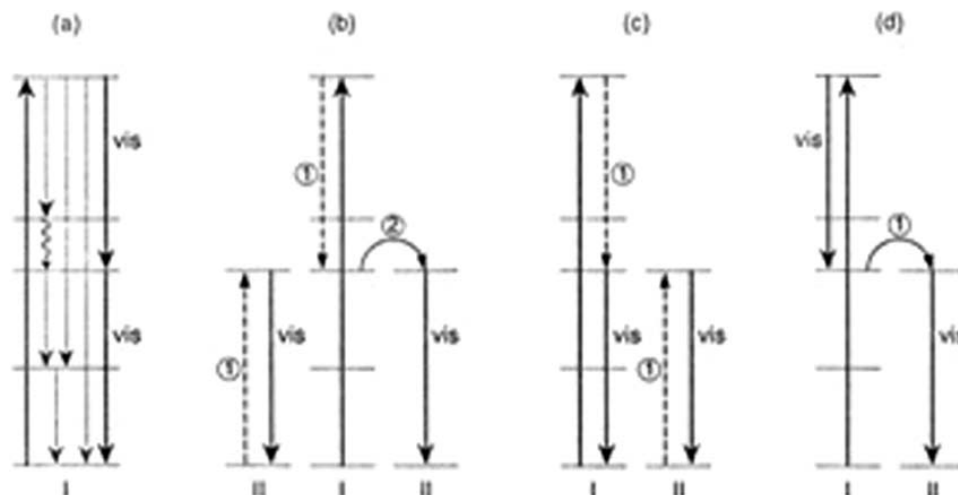
13

the pump light is strongly absorbed. Qualitatively, this process can occur under the following conditions: (1) the first absorption is weak, so the excitation should not be at the wavelength of the corresponding absorption peak, but at the tail of the absorption band; (2) the intermediate level has a long lifetime compared with the highest level; and (3) the cross-relaxation energy transfer between the highest level and the ground level is faster than any other relaxation mechanism. Figure 12 shows schematically the photon avalanche process in Tm^{3+}.

Finally, there are interesting advances in Monte Carlo modelling within this field, which can help to elucidate the emission mechanisms via the simulation of UC luminescence results.[114]

Down-conversion processes

In contrast to UC, down-conversion (DC) processes a high energy photon leads to the emission of visible or NIR photons (quantum cutting) (Fig. 13a).[115,116] In order to avoid ultraviolet and infrared emissions, energy transfer processes between the different ions are required (Fig. 13b–d).

One main application of this phenomenum is within the photovoltaic energy field (Fig. 14), since DC emissions avoid the current thermalisation losses in the crystalline silicon solar cells.[117] Yb^{3+} is the most used RE ion for this purpose, since it has an optical transition at about 1000 nm, just over the silicon gap. DC mechanisms involving Yb^{3+} ions are generally similar: a codopant RE ion acts as a sensitiser, receiving the excitation wavelength, generally in the blue range, then transferring energy to the Yb^{3+} ions, which act as activators, emitting about 1000 cm^{-1}. The visible emission of the sensitiser, generally in the range from green to red, is also obtained.

Luminescence, UC and DC in fluoride glasses and crystals

Phosphate glasses were the first studied hosts of RE ions[118–120] because of their idoneous refractive index, high transparency to ultraviolet light, high gain, good thermo-optical performance, low rupture strength and sufficient chemical durability. Schott Glass Technologies (USA) developed the glass LG-750, which is a well known commercial laser in the system P_2O_5–K_2O–BaO–Al_2O_3

doped with a significant amount of Nd_2O_3. The glass is of great significance in the market for high average energy and high peak power solid state laser applications (Ref. 121 and references Therein). The drawbacks of these systems are the short lifetime of the excited states and non-radiative decay paths. Fluoride glasses with low matrix vibrational energies have been further developed which enhance the efficiency of the radiative decay.

Within the fluoride and oxyfluoride glass systems, it is worth citing the review of Tran *et al.*[122] which is focused on heavy metal fluoride glasses and AlF_3 based glasses. Allen *et al.*[123] studied Tm^{3+} doped ZBLAN fibre glasses (ZrF_2–BaF_2–LaF_3–AlF_3–NaF) obtaining infrared emission from the excitation at 790 nm. By measuring the power output versus absorbed pump power at 790 nm, efficiencies of 35% were achieved. Murtagh *et al.*[124] described the phenomenum of laser cooling from the
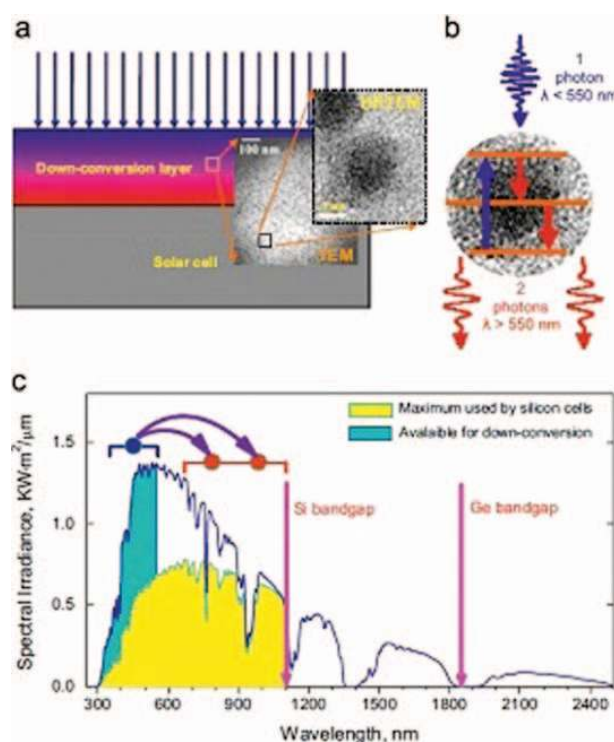
COLOUR FIGURE

14

fluorescence properties of Yb^{3+} doped ZBLANPb glasses. Temperature drops of 16 K have been observed in fibre samples.

Tanabe et al.[125] doped fluoride glasses with Tm^{3+}, relating the UC luminescence directly with the Judd–Ofelt parameters. Seeber et al.[126] dealt with Pr^{3+} doped fluorozirconates, fluorindates and fluorophosphates, and concluded that fluorozirconates are the most suitable matrices for applications in optical devices, since fluorindates tend to easily crystallise and fluorophosphates present a high photonic energy. They also focused on Nd^{3+} doped fluorophosphate glasses,[127] analysing the dependence of the Nd^{3+} emission at 1·06 μm on the chemical structure of the glass matrix.

One interesting field using glassy matrices is the generation of white light from multidoped glasses. Multicolour and white light can be achieved by combining the emission of the three primary colours, red, green and blue, from glasses doped with multiple RE ions. An optimum codoping strategy requires an energy transfer between the involved ions, so the emission radiation of one is absorbed for the other ion to be excited to a higher level, producing more intensive emission. Recently, Lakshminarayana et al.[128] developed Tm^{3+}/Dy^{3+} codoped oxyfluoridegermanate glasses, which show white light emission after excitation at 350 nm. These authors[129] also analysed the DC emission in oxyfluoride glasses of composition $50GeO_2–10B_2O_3–20ZnO–20LaF_3-0·5(RE)F_3.x$ $YbF3$ (RE=Pr, Tb, Tm; $x=0–30$ mol-%). Energy transfer from one of the codopant RE^{3+} ions to two Yb^{3+} ions leads to an infrared emission at 950–1100 nm, with efficiencies of 200%.

The sol–gel method offers the advantage of permitting the incorporation of a higher dopant concentration without loss of amorphous character. Doped fluoride glasses and crystals obtained by this method are reported in Refs. 130–132. Sol–gel materials are obtained as thin films and coatings, in contrast to bulk materials prepared by the melting method.

Concerning fluoride crystalline systems, the works of Hewes[133] and Guggenheim and Johnson[134] are of particular importance, in which the UC emissions of different RE ions in fluoride crystals are analysed. The observation of stimulated emission by UC at 77 K was reported in 1971 by Johnson and Guggenheim[135] in BaY_2F_8 codoped with Yb^{3+}/Er^{3+} and Yb^{3+}/Ho^{3+}. Joubert[109] summarised the RE doped materials in which PA has been observed, as well as crystalline UC lasers, in which $LaBr_3$, $LaCl_3$, LaF_3, $LiYF_4$, KYF_4, CdF_2 and CaF_2 are included.

LaF_3 is one of the most studied crystalline phases for doping with lanthanides. Weber[55] studied the $LaF_3:Er^{3+}$ system, whereas Collings and Silversmith[136] and Lim[137] treated the $LaF_3:Tm^{3+}$ material. The works of Chivian et al.[111] related to PA process in $Pr^{3+}:LaCl_3$ were followed by others with Sm^{3+}, Nd^{3+} and Tm^{3+} as doping agents in crystalline halides.[138–141] Macfarlane et al.[142] carried out UC measurements in crystalline fluorides doped with Er^{3+} and Nd^{3+}.

Mixed crystalline fluorides are becoming interesting because of the multisite nature of the crystalline lattice, meaning that RE ions can occupy various nonequivalent sites in the lattice; examples include $LiYF_4:Sm^{3+}$,[143] $KLaF_4:Sm^{3+}$,[144] $NaLaF_4:Ln^{3+}$ (Ln= Ce, Pr, Nd, Sm, Eu, Gd, Tb, Dy, Ho, Er, Tm)[145] and $NaLaF_4:Er^{3+}$.[146] The location of the energy levels of lanthanides ions by photo- and thermo-luminescence were studied in $NaGdF_4:Tm^{3+}$, $NaGdF_4:Nd^{3+}$, $NaLaF_4:Tm^{3+}$ and $NaLaF_4:Nd^{3+}$,[147] and $NaYF_4:Ln^{3+}$.[148,149]

Non-conventional methods have been used to obtain RE doped crystals including the core–shell method, where Diamente et al.[150] reported the development of core/shell nanoparticles of $LaF_3:Tm^{3+}/LaF_3$ which shows a high photoluminescence at 1·47 μm. Li et al.[151] employed hydrothermal synthesis to synthesise Eu^{3+} doped LnF_3 crystals in an aqueous medium, obtaining different morphologies. The coprecipitation method was used to obtain Eu^{3+} doped $NaGdF_4$ and $KGdF_4$ crystals.[152,153]

The main advantage of these works is the low vibrational energies of fluoride matrices. However, the high cost and the difficulty of obtaining extended crystalline matrices represents a real limit to scale-up of these materials.

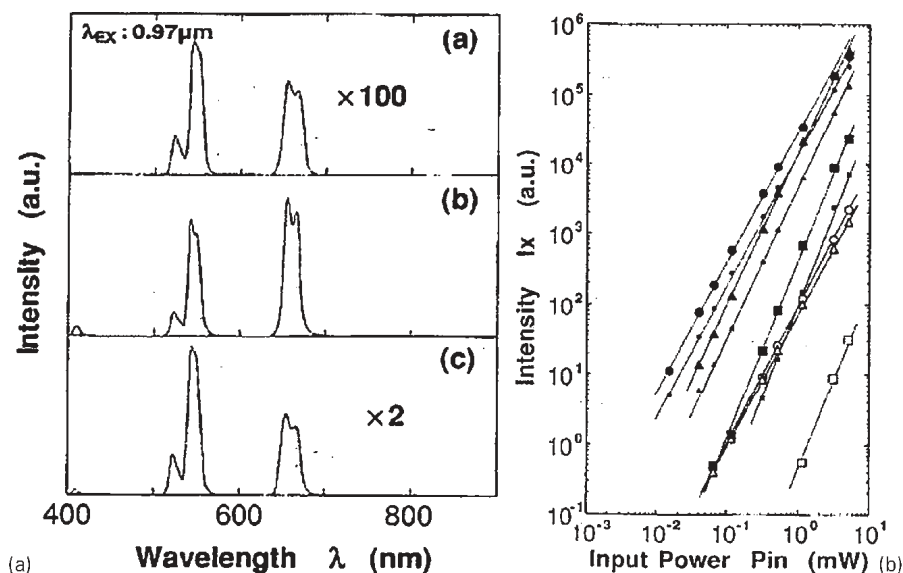## Luminescent processes in oxyfluoride glass ceramics

Wang and Ohwaki's composition

The first publication on oxyfluoride glass ceramics was by Wang and Ohwaki in 1993,[1] who reported the composition $30SiO_2–15Al_2O_3–20CdF_2–4PbF_2–10YbF_3–1ErF_3$ (mol-%). The authors ascribed the crystalline phase to $Pb_xCd_{1-x}F_2$, but further investigations suggested that their results could be compatible with PbF_2, CdF_2 or a $Pb_xCd_{1-x}F_2$ solid solution.

Two further works have played a decisive role to clarify this topic. Tikhomirov et al.[154] confirmed the crystallisation of PbF_2 from the glass composition $32SiO_2–12·5AlO_{1·5}–31·5CdF_2–18·5PbF_2–5·5ZnF_2–3·5ErF_3$ (mol-%), through EDS data, and suggested a model for nucleation and growth of this phase. The parent glass was heat treated at T_g (390°C) for 3 h, indicating the presence of 2·5 nm orthorhombic $PbF_2:Er^{3+}$ crystallites, which forms nucleation centres. When this glass ceramic is heat treated at temperatures above 350°C, the transformation from orthorhombic $PbF_2:Er^{3+}$ to cubic $PbF_2:Er^{3+}$takes place, and further heat treatment contributes to the growth of $PbF_2:Er^{3+}$cubic crystals. Er^{3+} occupies Pb^{2+} sites, creating a cation vacancy, which is charge compensated by additional F^- and resulting in distortion of the cubic fluorite structure. Beggiora et al.[155] attributed this controversy to the low crystalline fraction and line broadening of the X-ray peaks due to the nanometric size of the crystals. They studied the glass composition $30SiO_2–15Al_2O_3–29CdF_2–17PbF_2–5ZnF_2–4ErF_3$ (mol-%), through computer simulation methods, concording with Tikhomirov et al. with regard to an F^- interstitial compensation mechanism, in which Er^{3+} substitutes Pb in PbF_2 crystal; however, they further suggested a coexistence of cubic and trigonal structures, which could explain the distortion of the fluorite structure reported by Tikhomirov et al. Thus, these works show that Er^{3+} is located in a PbF_2 fluorite or distorted fluorite structure, rather than in the $Pb_xCd_{1-x}F_2$ solid solution reported by Wang and Ohwaki.

Recently, Hass et al.,[156] in collaboration with Rüssel, studied glass ceramics from the composition $21·1SiO_2–7Al_2O_3–6·5B_2O_3–14·3CdF_2–21·0PbF_2–11·0PbO–7·6CdO–11·0YbF_3–0·5ErF_3$ (mol-%) through anomalous small

International Materials Reviews imr175.3d 30/6/11 01:32:20
The Charlesworth Group, Wakefield +44(0)1924 369598 - Rev 7.51n/W (Jan 20 2003)

International Materials Reviews 2011 VOL 000 NO 000 11

$\lambda_{EX}: 0.97\ \mu m$

(a) ×100

(b)

(c) ×2

15

angle X-ray scattering. This work confirms the previous studies of Tikhomirov *et al.* and Beggiora *et al.*, concluding that the composition of the precipitated crystals in the glass ceramics obtained at 405°C during 30 min is $Pb_{17}Yb_{17}Er_2F_{64}$.
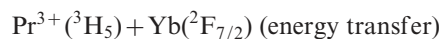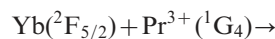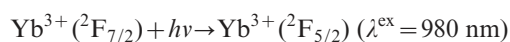
PbF_2 has a possess very low phonon energy, about 250 cm^{-1}, and doping with Yb^{3+}/Er^{3+} ions generates an UC emission which is more brilliant than those observed in the fluoride glass of composition $35AlF_3$–$14YbF_3$–$lErF_3$–$20PbF_2$–$5MgF_2$–$15CaF_2$–$10\ BaF_2$ (mol-%), which was the most efficient infrared UC material until 1993.[157] Figure 15 shows the UC spectra and the UC intensities of the precursor glass at 410, 550 and 660 nm after excitation at 972 nm; the glass ceramic and an alumino-fluoride glass are shown for comparison.

The use of amplifiers in the range $1\cdot3$–$1\cdot5\ \mu m$ triggered research on doped materials for optics waveguides. A $^1G_4 \rightarrow {}^3H_5$ transition of Pr^{3+} is used in most of these devices, but a main drawback is the high phonon energy of the oxide host. Thus, the use of oxyfluoride glass ceramics seems to be ideal.

Wang and Ohwaki's glass ceramic was the starting point for the design of matrices for Pr^{3+} ions to retain the transmission at 1300 nm, avoiding the presence of Yb^{3+}, which make this emission difficult. Tick *et al.*[158] substituted YbF_3 for YF_3 and for a mixture YF_3/ZnF_2 in glasses of composition $30SiO_2$–$15Al_2O_3$–$29CdF_2$–$17PbF_2$–$4YF_3$–$5ZnF_2$ and $30SiO_2$–$15Al_2O_3$–$29CdF_2$–$22PbF_2$–$4YF_3$ (mol-%). After heat treatment at around 470°C, from periods of a few minutes to more than 12 h, a crystalline phase of CdF_2 with a fluorite type structure precipitates and corresponds to CdF_2. Crystal sizes between 9 and 18 nm and a volume fraction of 20–30% were estimated from XRD and TEM. Evidence of the presence of Pr^{3+} ions in crystals is provided by the following: (1) after excitation at $1\cdot02\ \mu m$, glassy samples did not present fluorescence; (2) the lifetime of the transition $^1G_4 \rightarrow {}^3H_5$ (between 100 and 160 μs for Pr^{3+} concentrations from 150 to 900 ppm) is longer in the glass ceramics than that of the parent glass, increasing with increasing crystal fraction; and (3) Judd–Ofelt analysis shows that Ω_2 decreases from $0\cdot89$ before the heat

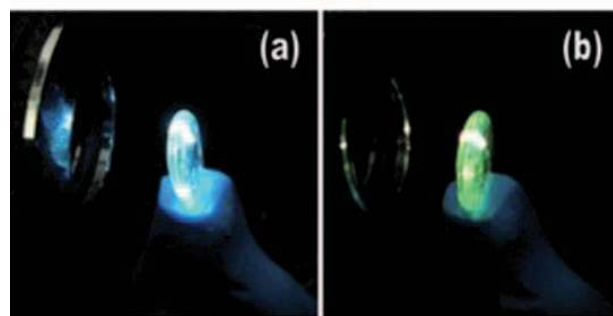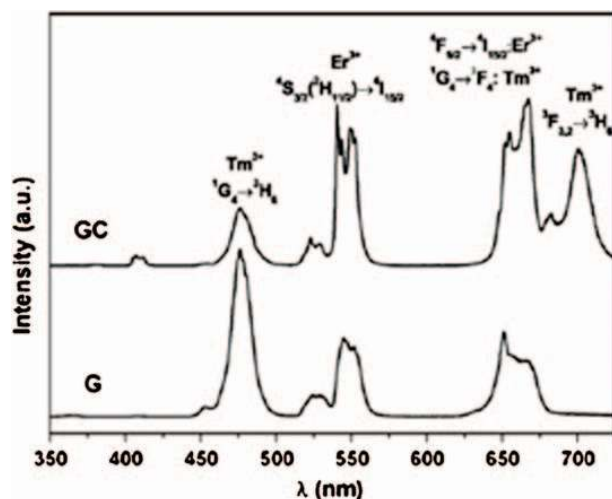treatment to $-0\cdot88$ in the glass ceramic, due to the higher ionic environment around the Pr^{3+} ions created by fluorine.

González Pérez *et al.*[159] studied a similar glass composition, codoped with Pr^{3+}/Yb^{3+}. Comparing the Judd–Ofelt parameters Ω_6 in the glass and glass ceramic, it can be estimated that around 80% of Pr^{3+} ions are located in the crystalline phase. Pr^{3+} emission at 1300 nm was detected under excitation at 980 nm, according to the following mechanism

$$Yb^{3+}(^2F_{7/2}) + h\nu \rightarrow Yb^{3+}(^2F_{5/2})\ (\lambda^{ex} = 980\ nm)$$

$$Yb(^2F_{5/2}) + Pr^{3+}(^1G_4) \rightarrow$$

$$Pr^{3+}(^3H_5) + Yb(^2F_{7/2})\ (energy\ transfer)$$

The energy transfer probability from Yb^{3+} to Pr^{3+} increases with phonon density, such that the Yb^{3+} and Pr^{3+} radiative emission intensities decrease. The authors consider the possibility of phonon assisted cross-relaxation channels affecting the $^1G_4$ level of Pr^{3+}. This work is a recent example of the open questions concerning the emission mechanisms and how external factors, such as temperature, provide useful information.

Tikhomirov *et al.*[160] analysed Er^{3+} doped glass ceramics of composition $32SiO_2$–$9AlO_{1.5}$–$31\cdot5CdF_2$–$18\cdot5PbF_2$–$5\cdot5ZnF_2$–$3\cdot5ErF_3$ (mol-%), by Raman spectroscopy, in which PbF_2 crystals of average size 13 nm form. The existence of predominant Q^2 units of F–Si–O tetrahedron as well as Q^0 units in the interphase crystal glass was proved. In a similar work, Er^{3+} was substituted for Tm^{3+},[161] in which it was possible to quantify that 57% of Tm^{3+} is located in a crystalline matrix. The quantity of RE ions located in crystals can also be estimated from emission spectra, as reported by Boulard *et al.*[162] in fluoride glass ceramics.

Apart from the infrared emission, Wang and Ohwaki's composition has been widely used to create materials producing visible emission through a UC mechanism. Takahashi *et al.*[163] doped Wang–Ohwaki's composition with Er^{3+}. After excitation at 800 nm, intensive emission bands at 550 and 660 nm are

12   **International Materials Reviews**   2011   VOL 000   NO 000

International Materials Reviews   imr175.3d   30/6/11   01:32:21
The Charlesworth Group, Wakefield +44(0)1924 369598 - Rev 7.51n/W (Jan 20 2003)

16

which only one photon process takes place in the Yb^{3+} emission, while two photons are involved in the Tm^{3+} emission process. From the UC emission spectrum at 475 nm, it is derived that 85% Tm^{3+} ions are incorporated into the crystalline phase in the $1Tm^{3+}$–$2\cdot5Yb^{3+}$ (mol-%) glass ceramic, but it is concluded that the Tm^{3+} optically active centres are those which are not in the fluoride nanocrystals. This is in good agreement with a phonon assisted energy transfer between Tm^{3+} and Yb^{3+}. However, this idea does not agree with that proposed by Zhang et al.[169] in Tm^{3+}/Yb^{3+} codoped glass and glass ceramic, in which the more intense UC emission in the glass ceramic, compared with that of the glass, is due to the crystalline surrounding of both ions, where the distances between them become shorter making the energy transfer processes easier. These results highlight the controversy concerning the UC mechanisms and the need for a complete structural characterisation of RE ions in glass ceramics.
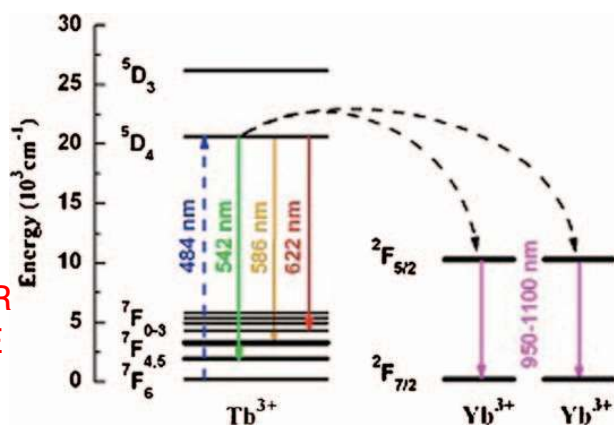
Tikhomirov et al.[170] and León-Luis et al.[171] studied $Yb^{3+}/Er^{3+}/Tm^{3+}$ codoped nanoglass ceramics. In the latter, the glass composition is $30SiO_2$–$15AlO_{1\cdot5}$–$29CdF_2$–$22PbF_2$–$1\cdot5YF_3$–$1\cdot5YbF_3$–$0\cdot5ErF_3$–$0\cdot5TmF_3$ (mol-%). A blue emission dominates the UC spectrum in the glass, while the green and red emissions are the most intense in the glass ceramic (after excitation at 980 nm) leading to a tuneable material (Fig. 16).

Méndez-Ramos et al.[172] studied a similar composition doped with Nd^{3+}, in which the Nd^{3+} is added through a alcoholic nitrate solution to the other raw materials, forming after the evaporation, a very fine powder. This powder was heated in a furnace at $1050°C$ for 1 h and the melt was poured onto a stainless steel plate at room temperature. Transparent oxyfluoride glass ceramics were obtained by thermal treatment of the precursor glass. In comparison to the conventional melting method, UC efficiency is lower in glass ceramics obtained by the solution method, because the greater dispersion of ions in the solution makes the energy transfer processes more difficult.

Rodríguez et al.[173] studied Yb^{3+}/Er^{3+} codoped PbF_2 glass ceramic obtained from a parent glass of composition $32SiO_2$–$9AlO_{1\cdot5}$–$31\cdot5CdF_2$–$18\cdot5PbF_2$–$5\cdot5ZnF_2$–$3\cdot5(Yb^{3+}/Er^{3+})F_3$ (mol-%). An exhaustive analysis of the DC mechanisms is put forward, based on the emissions at 378, 450 and 486 nm, developing blue to NIR photons. The DC efficiency reaches almost 200%.

In contrast to studies of the UC processes, no comparative results between precursor glasses and glass ceramics are found in publications concerning DC. Nevertheless, it would be useful to study the DC efficiency depending on the RE ion environment.

We summarise this section by restating that Wang and Ohwaki's composition is a fundamental starting point for the design of new doped glass ceramics, providing infrared, visible and tunable emissions by changing the dopant ion for each desired wavelength. It is necessary to know the energy level diagram of the used dopant ions, as well as their population processes and location in the crystalline phase. Several questions are still open concerning the emission mechanisms of the employed RE ions.

obtained. The Er^{3+} concentration dependence on UC intensity has been studied and a UC mechanism for both emission bands has been put forward.

Another variant of Wang–Ohwaki's glass ceramic is described by Kukkonen et al.[164] starting from composition of $30SiO_2$–$15Al_2O_3$–$29CdF_2$–$17PbF_2$–$3YF_3$–$5ZnF_2$ and $30SiO_2$–$15Al_2O_3$–$29CdF_2$–$22PbF_2$–$4ErF_3$–$5ZnF_2$ (mol-%). EDS spectra of the glass ceramics show an increase in the signal of Er^{3+} in the crystal phase and a subsequent decrease in the residual glass matrix.

A visible blue emission of Tm^{3+} has been widely studied due to its possible application in optical devices for high optical density storage,[165] visible lasers, optical amplifiers, colour display, undersea optical communications, sensors, and in the field of medicine for biomedical diagnostics.[166] Lahoz et al.[167] focused their studies on Tm^{3+}/Yb^{3+} codoped glass ceramics of composition $30SiO_2$–$15Al_2O_3$–$29CdF_2$–$22PbF_2$–$(4-x-y)YF_3$–$xTmF_3$–$yYbF_3$, with $x=0$, $0\cdot1$ and 1, and $y=0$ and $2\cdot5$. This work shows the advantages of an oxide environment for the RE ion, instead of an ordered fluoride one, since an UC mechanism based on an energy transfer via phonons is suggested. The effect of the host lattice in this codoped system was studied by Sommerdijk.[168] Absorption and excitation spectra of $0\cdot1Tm^{3+}$–$2\cdot5Yb^{3+}$ (mol-%) codoped glass and glass ceramic are coincident, due to the fact that two Tm^{3+} ions are involved in the blue UC emission, so the glass ceramic excitation spectra is the result of the overlap between two absorption spectra, $2Tm\,(^3H_6)\rightarrow2Tm\,(^3H_4)$. This has been demonstrated by the linear intensity dependence with pumping power of the bands at 475 nm (Tm^{3+}:$G_4\rightarrow^3H_6$) and 975 nm (Yb^{3+}:$^2F_{5/2}\rightarrow^2F_{7/2}$), in

International Materials Reviews   imr175.3d   30/6/11 01:32:23
The Charlesworth Group, Wakefield +44(0)1924 369598 - Rev 7.51n/W (Jan 20 2003)

International Materials Reviews   2011   VOL 000   NO 000   13

17

Other compositions

This section is focused on the crystallisation and luminescence properties of doped glass ceramics with crystalline phases which differ from that reported by Wang and Ohwaki. These compositions are classified by the precipitated crystalline phase: CaF_2, SrF_2, BaF_2, PbF_2, YF_3, LaF_3, $NaYF_4$ and $NaLaF_4$.

RF_2 ($R=Ca$, Sr, Ba, Pb)

All these crystalline phases possess a cubic fluorite type structure (space group $Fm\overline{3}m$), in which the R^{2+} cation is coordinated by eight fluoride anions and each F^- ion is surrounded by four R^{2+} ions.

CaF_2 exhibits a well known high transparency from 0·13 to 9·5 μm. The low phonon energy of CaF_2, around 280 cm^{-1},[174] has given rise to the continuous development of glass ceramics containing this crystalline phase.

Huang et al.[175] developed Yb^{3+} and Tb^{3+} codoped oxyfluoride glass ceramics of composition 47·4SiO_2–19Al_2O_3–28·4CaF_2–2TbF_3–3·2YbF_3 (mol-%). Emission bands at 381, 415 and 437 nm show a cubic dependence on the pump power at 974 nm, while those at 490, 546, 588 and 622 nm exhibit quadratic dependence, indicating that three and two photons are involved respectively. Energy transfer processes occur between both ions. Moreover, the longer lifetime of the $^5D_4$ level in the glass ceramics compared with that of the glass increases the excited state absorption of this level, which is involved in the mechanism. Ye et al.[176] also worked on Yb^{3+}/Tb^{3+} codoped glass ceramics, of composition 60SiO_2–20Al_2O_3–20CaF_2–0·3Tb^{3+}–xYb^{3+} ($x=0$, 4, 6, 10, 14, 18, 22, 26 and 30) (mol-%). After excitation at 484 nm, this material gives rise to an Yb^{3+} emission between 950 and 1100 nm (Fig. 17), which renders it suitable for DC applications. Recently, Lin et al.[177] have reported Tb^{3+}/Sm^{3+} codoped oxyfluoride aluminosilicate CaF_2 glass ceramics showing white light emission.

Chen et al.[178,179] developed glasses and glass ceramics of composition 44·5SiO_2–24·8Al_2O_3–5·0CaO–9·9NaF–14·8CaF_2 (mol-%) doped with different concentrations of Er^{3+}. The work reported in Ref. 179 facilitates studies focused on Er^{3+} doped systems as it provides a compilation of spectroscopic measurements based on Judd–Ofelt theory, showing the radiative transition probabilities, the fluorescence branching ratios and the radiative decay times of the studied glass and glass ceramics. Green and red UC emissions are present in the glass ceramics after excitation at 980 nm, whereas in the glasses, they were too weak and impossible to detect.

UC emission increases with Er^{3+} concentration up to 2 mol-%, where after concentration quenching occurs. Zhou et al.[180] obtained Er^{3+} doped glass ceramics containing CaF_2 nanocrystals by the sol–gel method. A red UC emission takes place in the glass ceramics after excitation at 980 nm.

SrF_2 possesses phonon energy of 400 cm^{-1}. Yu et al.[181] reported an Er^{3+} doped SrF_2 glass ceramic, which presents green and red UC emissions after excitation at 976 nm, and DC in the same range after excitation at 379 nm. BaF_2 exhibits phonon energy of 346 cm^{-1}. Qiao et al.[182] reported glass ceramics of composition 60SiO_2–17ZnF_2–20BaF_2–3ErF_3 (mol-%) in which BaF_2 is crystallised. Green and red UC luminescence is hardly observed in the glass upon excitation at 980 nm, whereas in the obtained glass ceramics, it is very intense, increasing with treatment time at 650°C. It is known that two phonons are involved in the mechanism from the UC intensity dependence on the pumping power. The suggested that mechanisms for both UC emissions in the glass ceramics include phonon decay processes, which is not expected for location of the Er^{3+} ions in a low phonon energy host such as BaF_2.[183]

Yu et al.[184] reported a glass of composition 68SiO_2–15BaF_2–13K_2CO_3–3La_2O_3–1Sb_2O_3–0·5ErF_3 (mol-%). The fluorescence lifetime of the Er^{3+} transition $^4I_{13/2} \rightarrow {}^4I_{15/2}$ in this material is remarkably longer, 13·39 ms, than that in other glasses and glass ceramics reported previously.

Li et al.[185] developed glasses and glass ceramics of composition 52SiO_2–20Al_2O_3–13Na_2O–5BaO–10BaF_2 (mol-%), codoped with 1 mol-%Yb_2O_3, 0·1 mol-%Tm_2O_3 and 0·1 mol-%Er_2O_3. Blue, green and red UC emissions are found under excitation at 980 nm, which are more intense in the glass ceramic material than in the corresponding glass, rendering this material suitable for generation of white light.

One of the few works which analyses the effect of RE ions on crystallisation is that of Rocha Barros et al.[186] The composition of the glasses is $(100-x)(7·52Al_2O_3$–15·04K_2O–1·88Na_2O–6BaF_2–69·63SiO_2)–$xBaO$ ($x=0$, 1·5, 3) (mol-%), doped with SmF_3 and ErF_3. The undoped glass is homogenous, while the doped glasses present phase separation droplets. These regions seem to control further crystallisation mechanism. Transparent Sm^{3+} and Er^{3+} doped glass ceramics do not exhibit significant differences in the fluorescence emission spectra in comparison with undoped glass ceramics, indicating that most of the RE ions are distributed in the glass matrix, instead of in the crystalline phase.

Chen et al.[187] reported glass ceramics of composition $xErF_3$–5BaF_2–95SiO_2 ($x=0$, 0·5, 1·0) (mol-%) obtained by the sol–gel method. Absorption spectra of the parent xerogel compared with the glass ceramics indicate a decrease in intensity of the hypersensitive transitions $^4I_{15/2}$–$^4G_{11/2}$ and $^4I_{15/2}$–$^2H_{11/2}$ in the glass ceramics with respect to those in the precursor glass, indicating an alteration of the Er^{3+} environment from amorphous silica to crystalline fluoride on crystallisation.

PbF_2 crystallisation in doped systems has also been reported in glass compositions different from those of Wang and Ohwaki. Duan et al.[188] obtained white light from a glass of composition 40SiO_2–10$AlO_{1·5}$–45PbF_2–5AlF_3 (mol-%), doped with Tm^{3+}, Er^{3+} and Yb^{3+}, under excitation at 970 nm. Zeng et al.[189] based their

18

19

COLOUR
FIGURE
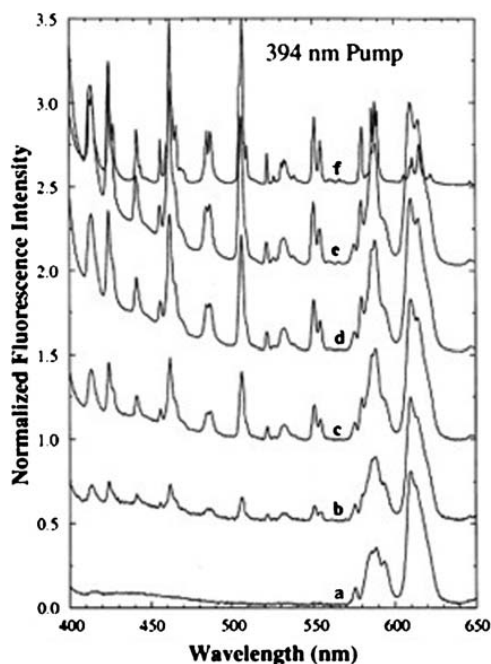
studies on Er^{3+} doped PbF_2 glass ceramics of composition $50SiO_2$–$20PbF_2$–$30PbO$–$0.5Er^{3+}$ (mol-%), where Er^{3+} ions act as nucleating agents.[190,191] Several sources of Er^{3+} have been used including Er_2O_3, $ErOF$, ErF_3 and $ErCl_3$. XRD peaks become sharper and more intense in the sequence $ErCl_3<Er_2O_3<ErOF<ErF_3$, showing that ErF_3 is the most suitable source.

RF_3 ($R = Y$, La)

At room temperature, YF_3 presents orthorhombic symmetry with space group Pmma β-YF_3. In this structure, the Y^{3+} ion lies in the centre of an irregular trigonal prism with six F^- ions at the corners. Three more fluorine ions are symmetrically disposed in front of the prism lateral faces. These polyhedra form rings of six prisms, four of which share faces and the others edges.

YF_3 crystals present phonon energy of 500 cm^{-1}. Nd^{3+} fluorescence emissions in YF_3 containing glass ceramics of composition $44SiO_2$–$28Al_2O_3$–$17NaF$–$11YF_3$ (mol-%) are prime candidates for laser applications in the visible and ultraviolet range.[192,193] Chen *et al.*[194] reported YF_3 glass ceramic codoped with Ho^{3+}, Tm^{3+} and Yb^{3+}, showing white light emission after excitation at 976 nm. Chen *et al.*[195] developed Pr^{3+}/Yb^{3+} codoped glass ceramics in the system SiO_2–Al_2O_3–NaF–YF_3, where β-YF_3 crystallised. From excitation at 482 nm of the $^3P_0$ level of the Pr^{3+} ion, emissions in the red and in the NIR range are obtained.

LaF_3 has a trigonal structure and crystallises in the tysonite structure ($P\bar{3}c1$) in which the site symmetry of La^{3+} is C_2. Dejneka[196] studied glass compositions in the range $(50$–$70)SiO_2$–$(0$–$13)Na_2O$–$(20$–$32)Al_2O_3$–$(0$–$9)La_2F_6$ (mol-%) with several RE ions as dopants. Depending on the composition, different lanthanide fluoride phases crystallise. Under 394 nm excitation, fluorescence of EuF_3 containing glasses and glass ceramics showed bands at 576, 590 and 612 nm, corresponding to $^5D_0\rightarrow^7F_0$, $^5D_0\rightarrow^7F_1$ and $^5D_0\rightarrow^7F_2$ transitions respectively. The ratio $^5D_0\rightarrow^7F_1/^5D_0\rightarrow^7F_2$ increases with increasing temperature of heat treatment, indicating that the Eu^{3+} sites become
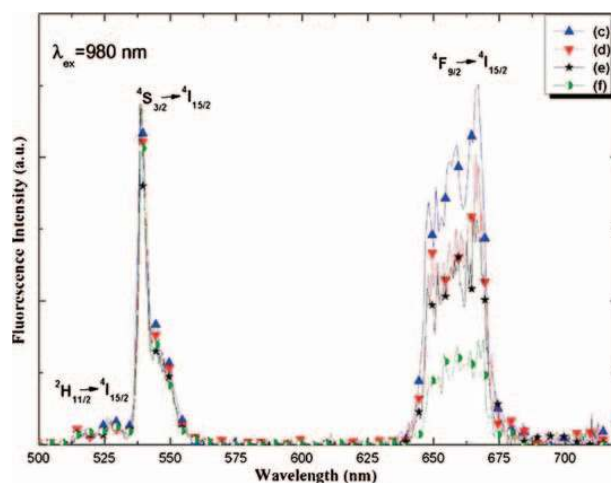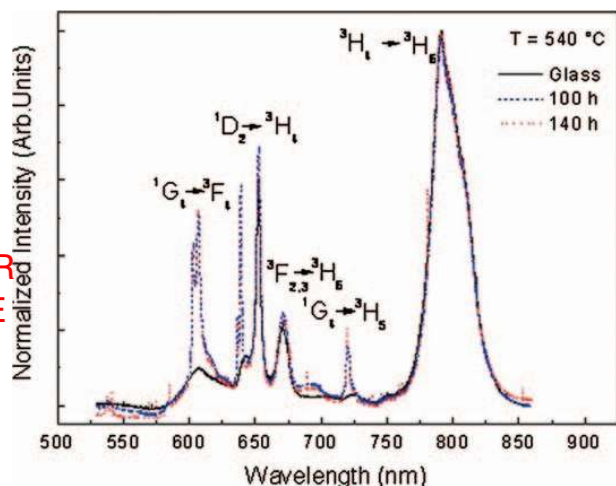
more symmetric (Fig. 18). Dejneka showed that the energy transfer between $^5D_3$, $^5D_2$, $^5D_1$ and $^5D_0$ takes place if the average distance between Eu^{3+} ions is shorter than 4 nm, so the change in the emission bands is evidence of the location of some Eu^{3+} into fluoride crystals.

Hu *et al.*[197] studied Er^{3+} doped glass ceramics with composition $41.2SiO_2$–$29.4Al_2O_3$–$17.6Na_2CO_3$–$11.8LaF_3$–$xErF_3$ ($x=0$, 0.5, 1, 2, 4, 6) (mol-%). From the displacements of DSC peaks of samples with different Er^{3+} concentrations, the activation energy E_a and Avrami exponent n were calculated by Chen's[198] and Ozawa's[199] equations. This work is one of the few which includes evidence of the effect of the doping agent on crystallisation. The crystal size changes with ErF_3 concentration. The a and c lattice parameters of the precipitated LaF_3 crystals also change with dopant concentration because of the incorporation of Er^{3+} into the crystalline lattice. Glass ceramics show great UC intensity in samples with higher crystallinity. The same composition has been doped with Yb^{3+},[200] which revealed that the linear emission intensity at 980 nm increases with Yb^{3+} concentration up to 4 mol-%, where quenching effects are present.

Ma *et al.*[201] also reported green and red UC emission in glasses of composition $41.2SiO_2$–$29.4Al_2O_3$–$17.6Na_2CO_3$–11.8 LaF_3–1.0 ErF_3 (mol-%), in which LaF_3 crystallised. Two main bands are associated with $^4F_{9/2}\rightarrow^4I_{15/2}$ (660 nm) and $^4S_{3/2}\rightarrow^4I_{15/2}$ (540 nm) transitions of Er^{3+} (Fig. 19). A reduction of the emission intensity of the 660 nm band with the treatment time at 650°C is observed, since the population on the $^4F_{9/2}$ level decreases with crystal growth. The authors proposed that interactions of the electronic states of RE ions in nanocrystals with the vibrational excitations of the surrounding glass medium and with the mixed vibrational modes of nanocrystallites, and the glass tend to be weaker with crystal size, so relaxation between $^4S_{3/2}$ and $^4F_{9/2}$ was more difficult, and the population on $^4F_{9/2}$ decreased. Moreover, the ratio of the integrated intensity of the red (660 nm) and green emission (540 nm) changes when the heating time increases, so it is a suitable method for controlling both emissions.

Ye *et al.*[202] reported LaF_3 glass ceramics of composition $45SiO_2$–$12Na_2O$–$23Al_2O_3$–$20LaF_3$–$0.5Tm^{3+}$–xYb^{3+} ($x=0$, 4, 8) (mol-%). After excitation at 468 nm, infrared

International Materials Reviews imr175.3d 30/6/11 01:32:34
The Charlesworth Group, Wakefield +44(0)1924 369598 - Rev 7.51n/W (Jan 20 2003)

International Materials Reviews 2011 VOL 000 NO 000 15

20

emission takes place through a cooperative energy transfer between a Tm^{3+} ion and two Yb^{3+} ions.

LaF$_3$ glass ceramics prepared by sol–gel method have been developed, notably by the group of del Castillo and Yanes,[31,32,203,204] who obtained doped glass ceramics by sol–gel, involving devitrification with an argon laser, which leads to the presence of crystals only in a small selected area.

Mixed fluorides

$NaYF_4$ with a phonon energy of 360 cm^{-1}, exists in two polymorphs at ambient temperature and pressure: the hexagonal $Na_{1.5}Nd_{1.5}F_6$ type structure and the cubic fluorite type structure, depending on the synthesis method. Liu *et al.*[205] studied the glass composition $40SiO_2$–$25Al_2O_3$–$18NaCO_3$–$10YF_3$–$7NaF$–$xErF_3$ ($x=$ 0·05, 0·2, 0·5, 1·0, 2·0) (mol-%), in which the main characteristic is the transition from cubic α-$NaYF_4$ to hexagonal β-$NaYF_4$ when the temperature increases. β-$NaYF_4$ seems to be more efficient in luminescence processes than the α structure, due to the multisite nature of the Y^{3+}/RE^{3+} ions in the hexagonal $NaYF_4$ crystal.[206,207] This kind of polymorphism was also reported for $NaGdF_4$:Eu^{3+}, obtained by hydrothermal synthesis.[208] Yanes *et al.*[209] also developed $NaYF_4$ glass ceramics, codoped with Er^{3+}/Yb^{3+}, by the sol–gel method.

$NaLaF_4$ crystallises in the space group $P\bar{6}$ and has two La^{3+} sites, which are randomly occupied by the dopant ions. Both sites have tricapped trigonal prismatic coordination, one with C_{3h} and the other with C_1 site symmetry. The phonon energy is around 290 cm^{-1}. de Pablos-Martin *et al.*[210] reported an analysis of $NaLaF_4$ nanocrystallisation within an aluminosilicate matrix doped with Tm^{3+}. This work compares the undoped glass and glass ceramic in Ref. 96. with the Tm^{3+} doped analogues. Crystal sizes of the undoped glass ceramics are quite similar to those of 0·7%Tm^{3+} doped glass ceramic treated at similar temperatures but for much longer times, indicating that the maximum crystal size is reached faster in the undoped glass ceramics. It is concluded, therefore, that the addition of Tm_2O_3 gives rise to a delay in the crystallisation process. The limitation in the crystal growth is related to the formation of a barrier diffusion layer around the crystals, as reported in Ref. 96. Emission spectra after excitation at 488 nm of the precursor glass and different

glass ceramics are shown in Fig. 20. Additional and narrower bands appear in the glass ceramics in comparison with the parent glass, indicating the distribution of Tm^{3+} ions between both phases.

Zhao *et al.*[211] reported Ba_2GdF_7 nanocrystals containing glass ceramics, codoped with Eu^{3+}, Tm^{3+} and Yb^{3+}. This material shows white light emission under excitation at 392 nm.

Possible applications of doped nanocrystalline glass ceramics

Two main applications of oxyfluoride nanoglass ceramics have been reported in this review:

(i) UC and white light generation waveguides
(ii) DC materials, especially useful for the improvement of solar cells.

UC materials

Waveguides

The number of works studying the production of waveguides from glass ceramic materials is very low,[212,213] especially those focused on oxyfluoride systems.

Since the concept of internal reflection was developed in the nineteenth century, light guiding has advanced to a point where it has revolutionised information technology. Nowadays, it is required for medical applications and the transmission of information over long distances, including telephony, Internet traffic, long high speed local area networks, cable TV, etc.[214,215] The incorporation of RE ions into waveguides created a significant interest in finding materials which cover the broad available bandwidth of the spectra required for optical communications. Nowadays, Er^{3+} and Tm^{3+} doped fibres are useful in the third window of the spectra, since the emission occurs at 1·54 μm for Er^{3+} and between 1·450 and 1·480 μm for Tm^{3+}, while Pr^{3+} doped fibres operate in the second window, at 1·3 μm. Attenuation along the waveguide is one of the main factors impacting on the design of the material. Current efforts are focused on finding materials with propagation losses lower than 0·1 dB cm^{-1}. A major improvement in this area was the achievement of efficient pump beam propagation in the core of the fibre, and the subsequent gain, directly amplifying the output optical signal,[216] and avoiding the use of intermediate electronic devices. The largely suppressed multiphonon transitions in fluoride environments are very important for the fabrication of fibre lasers and amplifiers; thus oxyfluoride glass ceramics are very good candidates for these devices.

In 1969, Bell Laboratories developed the first optical integrated circuit, in which various components are interconnected with optical waveguides on a substrate, referred to as an integrated optical device (IODs). The advantages of using IODs compared with a long doped fibre are the lower cost and the decrease of interactions between RE ions. Jacquier *et al.*[217] has reviewed the main properties of RE doped fibres and IODs.

The ion exchange technique[218,219] (Fig. 21) is used to obtain waveguiding regions by exchanging certain cations from the glass for cations from a salt melt solution.[220] Changes in polarisability and molar volume result in zones of higher refractive index, where the light is confined. Structural changes produced by ion exchange process are detailed by Brandenburg[221] and

21
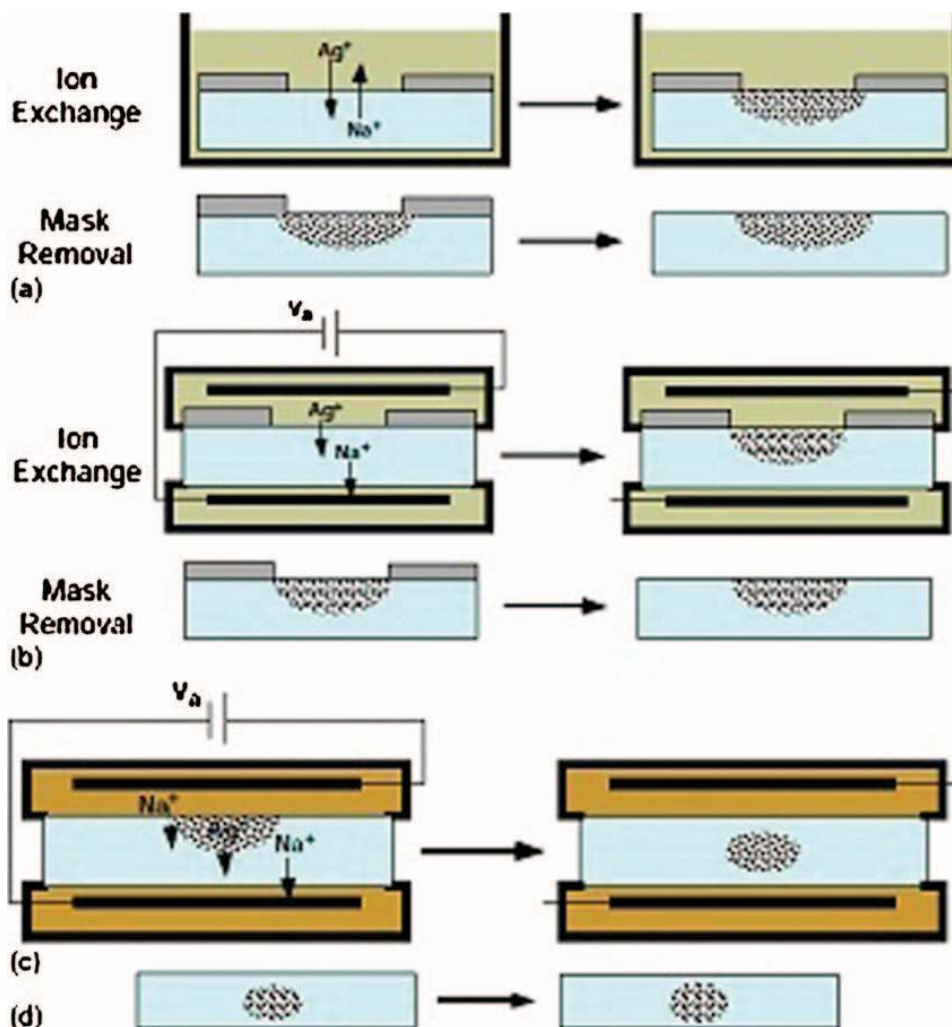
COLOUR
FIGURE

later Tyagi and Varshneya[222] Silver–sodium exchange has been particularly well studied,[223] especially the formation of Ag clusters, which give the characteristic yellow colour in the glass samples.[224] Ag particles are detectable by absorption measurements, showing a plasmon resonance at around 400 nm. Portales *et al.*[225] reported important results showing an enhancement of the $1 \cdot 5$ μm luminescence in annealed Er^{3+} doped Ag exchanged silicate glasses when the excitation wavelength is similar to that of the Ag plasmon absorption band. Righini *et al.*[226] and Berneschi *et al.*[227] have detailed similar effects.

The number of optical modes is defined by changing the ion concentration of the salt melt solution and the temperature and time of the ion exchange process. Typically, for amplification purposes in the infrared region, single mode waveguides are used, while for UC materials, in which high energy photons are produced, several modes are needed.

In principle, the use of glass ceramics in this field could be a disadvantage, since the crystals would contribute to light scattering.[228] On the other hand, when electrical control of light propagation or high non-linearity is necessary in optical waveguides, the presence of crystals in a glassy matrix is favourable. Thus, an exhaustive control of the crystallisation process must be developed in order to obtain ultra transparent glass ceramics with a homogenous size distribution of nanocrystals with particle size of only a few nanometres in order to avoid light scattering. Usually, work focused on the preparation of glass ceramic waveguides starts from the parent glasses and employs thermal treatment during ion exchange to produce the glass ceramics.[229,230] To our knowledge, not many syntheses start directly from the glass ceramic materials.

Photovoltaics

Richards[231] described the advantages of applying UC to photovoltaics for the following reasons: (1) visible light is achieved, with higher energy than that of the band gap E_g of Si solar cells; (2) an UC layer can be placed upon the rear of a bifacial solar cell without disturbing the performance of the device for incident photons with energy $E > E_g$; and (3) with a reflector placed behind the UC layer, no luminescence can escape out of the rear. On the other hand, the major disadvantage of UC is that it is a non-linear optical process. Thus, for the minimum two-step UC process, the intensity of UC light I is related to the incident light intensity I_0 by I/I_0^2, while for a three-step UC process, it is I/I_0^3.

DC materials

Zhang and Huang[116] reviewed NIR quantum cutting glass-ceramics containing BaF_2, CaF_2, TbF_3, LaF_3 and YF_3 nanocrystals. This work states that there are still many areas to be improved, highlighting the need for a

better understanding of material properties, fabrication processes and DC mechanisms. They concluded that a great number of newer concepts and novel materials are still in the research stage, which will lead to much higher efficiency and lower costs in the coming decades.

In contrast to RE doped glasses and crystalline phases,[112] RE doped glass ceramic materials are still not near to market in optics or photovoltaic applications. However, intensive research is currently focused on finding the best experimental conditions in order to achieve a higher crystalline fraction, maintaining the transparency, locating the majority of the RE ions in the crystalline phase, minimising the propagation losses and improving the optical emission rates. There exist a great number of possibilities in these fields, since several crystalline phases and RE ions are involved, where combination could be of interest. Richards[232] reported the requirements and limitations of luminescent materials for in-lighting, display and photovoltaic applications. The main challenges are: (1) higher stability, to avoid the formation of defects (fluorides are known to be damaged by vacuum ultraviolet radiation, reducing the efficiency of the luminescence); (2) higher emission lifetime, to increase the efficiency of luminescent processes; (3) the high price of RE minerals and the necessary purification process for lanthanides remains a barrier; and (4) reflection of the host material must be minimised in order to focus the light into the excited levels of the RE ions.

Conclusions

The general principles of nanocrystallisation in glasses have been reviewed with especial attention paid to the crystallisation of fluoride phases. Two different trends, which attempt to analyse the nanocrystallisation mechanisms, have been discerned. The base outlined by Stoch and Sroda *et al.* should be considered in the first stages of crystallisation, since they are based on theoretical aspects, such as crystallisation enthalpies, bond ionicities, heat capacities and thermal stability indices, allowing the crystallisation mechanism to be predicted. However, to complete these studies, a deeper knowledge of the structure and composition of the interphases formed between glass matrix and crystal, their evolution during crystallisation and the percolation theory, as suggested by Rüssel *et al.* is necessary. Both approaches represent the foundations for a better understanding of crystallisation phenomena in non-isochemical systems in general.

Nanocrystallisation has been successfully developed and transferred to the market for telescope mirrors, cook panels and fireplaces. However, the most relevant and recent publications concern optically active materials, in which the advantages of using RE doped oxyfluoride glass ceramics are put forward. Since Wang and Ohwaki reported their glass ceramics in 1993, changes in the original composition with different crystalline phases and dopant ions have been investigated. LaF_3 is an extensively studied fluoride, although recent investigations are focused on heavy fluorides, like PbF_2, and double fluorides, especially $NaYF_4$. More information about the influence of the addition of RE ions on crystallisation is needed by comparing doped and undoped systems.

Oxyfluoride glass ceramics offer an immense range of possibilities, for not only various compositions, crystalline phases and dopanting parameters, but also the final shape of the material. These include waveguides for IODs produced by melting, coatings and thin films made by sol–gel, nanoparticles, fibres, spherical devices, etc. From our point of view, finding the best material requires improvement of several factors: crystallisation of the appropriate fluoride crystal and doping with the ideal RE ion, a high crystalline fraction and maximum incorporation of the RE ion into the crystalline structure, costs of the raw materials, etc. These could be the reasons for the delay in the application of such materials in commercial devices, compared with the current glassy and crystalline analogues. This review has highlighted the importance of a complete understanding of the mechanisms of nucleation and crystallisation of fluoride nanocrystals in glasses.

The mechanisms that control the optical emissions have been reported, especially different kinds of energy transfer processes between excited states, giving rise to up- and down-conversion phenomena.

The perspectives of these materials represent a promising future for a great number of applications, especially in optics and photovoltaics.

Acknowledgements

References

1. Y. Wang and J. Ohwaki: *Appl. Phys. Lett.*, 1993, **63**, 3268.
2. G. Tammann: 'Der Glaszustand'; 1933, Leipzig, L. Voss.
3. A. K. Jackson: *Ind. Eng. Chem.*, 1965, **54**, (12), 29–32.
4. R. L. Thakur, K. Takijawa, T. Sakaino and T. Moriya: *Glass Ceram. Res. Inst. Bull.*, 1964, **1**, 1–22.
5. D. Turnbull and M. A Cohen: 'Crystallisation kinetics and glass formation', in 'Modern aspects of the vitreous state', (ed. J. D. Mackenzie), 1; 1960, Washington, DC, Butterworth Inc.
6. D. R. Uhlmann and B Chalmers: *Ind. Eng. Chem.*, 1965, **57**, (9), 19–31.
7. J. J. Hammel: 'Nucleation in glass. A review', in 'Advances in nucleation and crystallisation in glasses'; 1971, Columbus, OH, American Ceramic Society.
8. S. Toschev and I. Gutzow: *Phys. Status Solidi*, 1967, **21**, 683.
9. B. Hinz: *Silikattechnik*, 1960, **11**, (10), 455–459.
10. H. R. Lillie: *Glass Technol.*, 1960, **1**, (3), 115–120.
11. O. Robredo: *Verres Réfract.*, 1962, **16**, (4), 225–230; (5), 282–289.
12. M. Tashiro: *Glass Ind.*, 1966, **47**, 366–373, 428–435.
13. McMillan: 'Glass-ceramics', 1964, London/New York, Academic Press.
14. K. D. Kim and S. H. Lee: *J. Non-Cryst. Solids*, 2004, **336**, 195–201.
15. H. E. Kissinger: *J. Res. Natl Bur. Stand.*, 1956, **57**, 217–221.
16. Y. Senol, T. Osman and Ozkan: *Ceram. Int.*, 1996, **22**, 477–481.
17. M. Poulain: *J. Non-Cryst. Solids*, 1992, **140**, 1–9.
18. M. Avrami: *J. Chem. Phys.*, 1939, **7**, 1103.
19. M. Avrami: *J. Chem. Phys.*, 1940, **8**, 212.
20. M. Avrami: *J. Chem. Phys.*, 1941, **9**, 177.
21. W. A. Johnson and R. F. Mehl: *Trans. Am. Inst. Miner. Metall. Eng.*, 1939, **135**, 416.
22. B. N. Kolmogorov: *Izv. Akad. Nauk. URSS Ser. Mater.*, 1937, **3**, 355.

6

23. L. A. Pérez-Maqueda, J. M. Crudo and J. Malek: *J. Non-Cryst. Solids*, 2003, **320**, 84–91.
24. S. D. Stookey: *Res. Manage.*, 1958, **1**, (3), 155–163.
25. S. D. Stookey: 'Catalyzed crystallisation of glass, in theory and practice', *Ind. Eng. Chem.*, 1959, **1**, 805.
26. S. Bhattacharyya, Th. Höche, K. Hahn and P. A. van Aken: *J. Non-Cryst. Solids*, 2009, **355**, (6), 393–396.
27. W. Vogel: 'Glass chemistry', 2nd edn, 291; 1994, Berlin, Springer-Verlag.
28. B. Li, Z. X. Yue, J. Zhou, Z. L. Gui and L. T. Li: *Mater. Lett.*, 2002, **54**, 25–29.
29. S. Cai, W. J. Zhang, G. H. Xu, J. Y. Li, D. M. Wang and W. Jiang: *J. Non-Cryst. Solids*, 2009, **355**, 273–279.
30. Q.-Z. Chen, Y. Li, L.-Y. Jin, J. M. W. Quinn and P. A. Komesaroff: *Acta Biomater.*, 2010, **6**, 4143–4153.
31. J. J. Velázquez, A. C. Yanes, J. del Castillo, J. Méndez-Ramos and V. D. Rodríguez: *J. Non-Cryst. Solids*, 2010, **356**, 1349–1353.
32. A. C. Yanes, J. J. Velázquez, J. del Castillo, J. Méndez Ramos and V. D. Rodríguez: *J. Sol–Gel Sci. Technnol.*, 2009, **51**, 4–9.
33. L. Stoch: *J. Therm. Anal. Calorim.*, 1998, **54**, 9.
34. M. Sroda, I. Waclawska, L. Stoch and M. Reben: *J. Therm. Anal. Calorim.*, 2004, **77**, 193–200.
35. I. Avramov, R. Keding and C. Rüssel: *J. Non-Cryst. Solids*, 2000, **272**, 147–153.
36. I. Avramov, R. Keding, C. Rüssel and R. Kranold: *J. Non-Cryst. Solids*, 2000, **278**, 13–18.
37. R. P. F. de Almeida, C. Bocker and C. Rüssel: *Chem. Mater.*, 2008, **20**, 5916–5921.
38. I. Avramov, R. Keding and C. Rüssel: *Glass. Sci. Technol.*, 2000, **73C1**, 138–145.
39. R. G. Hill, M. D. O'Donnell, R. V. Law, N. Karpukhina, B. Cochrane and D. U. Tulyaganov: *J. Non-Cryst. Solids*, 2010, **356**, 2935–2941.
40. C. Rüssel: *Chem. Mater.*, 2005, **17**, 5843–5847.
41. I. Avramov, R. Keding, C. Rüssel and R. Kranold: *J. Non-Cryst. Solids*, 2000, **278**, 13–18.
42. I. Avramov, A. Milchev and P. Argyrakis: *Phys. Rev. E*, 1993, **47E**, (4), 2303.
43. N. Tsakiris, P. Argyrakis and I. Avramov: *Phys. Rev. E*, 2010, **81E**, 022101.
44. N. Tsakiris, P. Argyrakis, I. Avramov, C. Bocker and C. Rüssel: *Europhys. Lett.*, 2010, **89**, 18004.
45. M. J. Pascual, C. Lara and A. Durán: *Eur. J. Glass Sci. Technol. B*, 2006, **47B**, (5), 572–581.
46. I. W. Donald: *J. Non-Cryst. Solids*, 2004, **345**, 120–126.
47. M. J. Pascual, C. Lara and A. Duran: *J. Glass Sci. Technol. B*, 2006, **47B**, (5), 572–581.
48. A. Stamboulis, R. G. Hill and R. V. Law: *J. Non-Cryst. Solids*, 2005, **351**, 3289–3295.
49. T. J. Kiczenski and J. F. Stebbins: *J. Non-Cryst. Solids*, 2002, **306**, 160–168.
50. W. A. Pisarski, J. Pisarska, M. Mączka, R. Lisiecki, Ł. Grobelny, T. Goryczka, G. Dominiak-Dzik and W. Ryba-Romanowski: *Spectrochim. Acta A*, 2011, to be published.
51. C. Bessada, A. Rakhmatullin, A. L. Rollet and D. Zanghi: *J. Fluor. Chem.*, 2009, **109**, 45–52.
52. D. Furniss, E. A. Harris and D. B. Hollis: *J. Phys. C: Solid State Phys.*, 1987, **20C**, L147–L150.
53. B. Sreedhar, P. Indira and A. K. Bhatnagar: 'EPR spectra of transition metal and rare-earth ions in lithium fluoroborate glasses', Proc. AIP Conf.: 'Ordering disorder: prospect and retrospect in condensed matter physics', Hyderabad, India, December–January1992, AIP, Vol. 286, 258–260.
54. M. Takahashi, R. Kanno and Y. Kawamoto: J. Phys. Chem., 1996, **100**, (26), 11193–11197.
55. M. J. Weber: *Phys. Rev.*, 1967, **157**, (2), 262–272.
56. B. R. Judd: *Phys. Rev.*, 1962, **127**, 750–761.
57. G. S. Ofelt: *J. Chem. Phys.*, 1962, **37**, 511–520.
58. R. Moncorgé: in 'Spectroscopic properties of rare earths in optical materials', Springer Series in Materials Science, Vol. 83, 320–378; 2005, Berlin, Springer.
59. M. C. Gonçalves, L. F. Santos and R. M. Almeida: *C. R. Chim.*, 2002, **5**, 12, 845–854.
60. M. M. Lezhnina, H. Kaetker and U. H. Kynast: *Opt. Mater.*, 2007, **30**, 264–272.
61. F. Lahoz, I. R. Martín, U. R. Rodríguez-Mendoza, I. Iparraguirre, J. Azkargorta, A. Mendioroz, R. Balda, J. Fernández and V. Lavín: *Opt. Mater.*, 2005, **27**, 1762–1770.
62. A. Edgar, G. V. M. Williams and J. Hamelin: *Curr. Appl. Phys.*, 2006, **6**, 355–358.

63. T. Döhring, R. Jedamzik, V. Wittmer and A. Thomas: *Proc. SPIE*, 2004, **5494**, 340–349.
64. T. Döhring, R. Jedamzik and P. Hartmann: *Proc. SPIE*, 2007, 6689.
65. T. Döhring, R. Jedamzik, A. Thomas and H. Morian: *Proc. SPIE*, 2003, **4851**, 647–655.
66. G. H. Beall and D. A. Duke: *J. Mater. Sci.*, 1969, **4**, 340–352.
67. G. H. Beall and L. R. Pinckney: *J. Am. Ceram. Soc.*, 1999, **82**, 5–16.
68. P. Riello, P. Canton, N. Comelato, S. Polizzi, M. Verità, G. Fagherazzi, H. Hofmeister and S. Hopfe: *J. Non-Cryst. Solids*, 2001, **288**, 127–139.
69. X. Z. Guo, H. Yang, M. Cao, C. Han and F. F. Song: *Trans. Nonferr. Met. Soc. China*, 2006, **16**, 593–597.
70. R. Wurth, F. Muñoz, M. Müller and C. Rüssel: *Mater. Chem. Phys.*, 2009, **116**, 433–437.
71. S. Bhattacharyya, T. Höche, J. R. Jinschek, I. Avramov, R. Wurth, M. Müller and C. Rüssel: *Cryst. Growth Des.*, 2010, **10**, 379–385.
72. F. Gabel, W. Kiefer, G. Müller, W. Pannhorst and R. Sprengard: *Glastech. Ber. Glass Sci. Technol.*, 2000, **73**, (C1), 337.
73. R. Sprengard, U. Fotheringham, W. Pannhorst and K. Binder: http://www.schott.com/rd/german/download/zusammensetzung12.pdf
74. K. Soga, W. Wang, R. E. Riman, J. B. Brown and K. R. Mikeska: *J. Appl. Phys.*, 2003, **93**, 2946.
75. D. W. Hewak, R. S. Deol, J. Wang, G. Wylangowski, J. A. Mederios Neto, B. N. Samson, R. I. Laming, W. S. Brocklesby, D. N. Payne, A. Jha, M. Poulain, S. Otero, S. Surinach and M. D. Baro: *Electron. Lett.*, 1993, **29**, 237.
76. E. R. Taylor, L. N. Ng, N. P. Sessions and H. Buerger: *J. Appl. Phys.*, 2002, **92**, 112.
77. Joint Committee on Powder Diffraction Standards (JCPDS) file 8-461 LaF$_3$
78. M. Sroda and Cz. Paluszkiewicz: *Vib. Spectrosc.*, 2008, **48**, 246–250.
79. M. Sroda, Cz. Paluszkiewicz, M. Reben and B. Handke: *J. Mol. Struct.*, 2005, **744–747**, 647–651.
80. M. Reben, I. Waclawska, Cz. Paluszkiewicz and M. Sroda: *J. Therm. Anal. Calorim.*, 2007, **88**, (1), 285–289.
81. N. Hémono, G. Pierre, F. Muñoz, A. de Pablos-Martín, M. J. Pascual and A. Durán: *J. Eur. Ceram. Soc.*, 2009, **29**, 2915–2920.
82. S. Bhattacharyya, Th. Höche, N. Hemono, M. J. Pascual and P. A. van Aken: *J. Cryst. Growth*, 2009, **311**, 4350–4355.
83. F. Muñoz, A. de Pablos-Martín, N. Hémono, M. J. Pascual, A. Durán, L. Delevoye and L. Montagne: *J. Non-Cryst. Solids*, 2011, **357**, 1463–1468.
84. R. E. Youngman and M. J. Dejneka: *J. Am. Ceram. Soc.*, 2002, **85**, 1077–1082.
85. T. J. Kiczenski, L.-S. Du and J. F. Stebbins: *J. Non Cryst. Solids*, 2004, **337**, 142–149.
86. J. F. Stebbins and Q. Zeng: *J. Non Cryst. Solids*, 2000, **262**, 1–5.
87. K. Ritter, S. Gerlach and C. Rüssel: *J. Non-Cryst. Solids*, 2010, **356**, 3090–3094.
88. C. Bocker and C. Rüssel: *J. Eur. Ceram. Soc.*, 2009, **29**, 1221–1225.
89. C. Bocker, S. Bhattacharyya, T. Höche and C. Rüssel: *Act. Mater.*, 2009, **57**, 5956–5963.
90. S. Bhattacharyya, C. Bocker, T. Heil, J. R. Jinschek, T. Höche, C. Rüssel and H. Kohl: *Nano Lett.*, 2009, **9**, (6), 2493–2496.
91. C. Bocker, F. Muñoz, A. Durán and C. Rüssel: *J. Solid State Chem.*, 2011, **184**, (2), 405–410.
92. C. Bocker, I. Avramov and C. Rüssel: *Chem. Phys.*, 2010, **369**, 96–100.
93. C. Bocker, I. Avramov and C. Rüssel: *Scr. Mater.*, 2010, **62**, 814–817.
94. F. Liu, Y. Wang, D. Chen and Y. Yu: *Mater. Sci. Eng. B*, 2007, **B136**, 106–110.
95. M. Sroda: *J. Therm. Anal. Calorim.*, 2009, **97**, 239–243.
96. A. de Pablos-Martín, G. C. Mather, F. Muñoz, S. Bhattacharyya, T. Höche, J. R. Jinschek, T. Heil, A. Durán and M. J. Pascual: *J. Non-Cryst. Solids*, 2010, **356**, 3071–3079.
97. G. Liu and B. Jacquier: in 'Spectroscopic properties of rare earths in optical materials', Springer Series in Materials Science, Vol. 83; 2005, Beijing, Springer.
98. J. F. Suyver, A. Aebischer, D. Biner, P. Gerner, J. Grimm, S. Heer, K. W. Krämer, C. Reinhard and H. U. Güdel: *Opt. Mater.*, 2005, **27**, 1111–1130.
99. Y. Cong, B. Li, B. Lei, X. Wang, C. Liu, J. Liu and W. Li: *J. Lumin.*, 2008, **128**, 105–109.

100. P. A. Azeem, M. Kalidasan, K. Rama Gopal and R. R. Reddy: *J. Alloys Compd*, 2009, **474**, 536–540.

101. B. C. Jamalaiah, J. Suresh Kumar, A. Mohan Babu, L. Rama Moorthy: *J. Alloys Compd*, 2009, **478**, 63–67.

102. Z. Lu, J. Wang, Y. Tang and Y. Li: *J. Solid State Chem.*, 2004, **177**, 3075–3079.

103. Z. Wang, M. Li, Ch. Wang, J. Chang, H. Shi and J. Lin: *J. Rare Earths*, 2009, **27**, (1), 33.

104. X. Qiao, Q. Luo, X. Fan and M. Wang: *J. Rare Earth*, 2008, **26**, (6), 883.

105. P. Babu and C. K. Jayasankar: *Physica B*, 2000, **279B**, 262–281.

106. R. Reisfeld, E. Zigansky and M. Gaft: *Mol. Phys.*, 2004, **102**, 1319–1330.

107. K. Binnemans, K. van Herck and C. Gorller-Walrand: *Chem. Phys. Lett.*, 1997, **266**, 297–302.

108. H. W. Leverenz: 'Introduction to luminescence of solids', 1968, New York, Dower Publications.

109. F. Auzel: *Chem. Rev.*, 2004, **104**, 139–173.

110. P. L. Dexter: *J. Chem. Phys.*, 1963, **21**, 876.

111. J. S. Chivian, W. E. Case and D. D. Eden: *Appl. Phys. Lett.*, 1979, **35**, 124.

112. M. F. Joubert: *Opt. Mater.*, 1999, **11**, 181–203.

113. S. Guy, M. F. Joubert and B. Jacquier: *Phys. Rev. B*, 1997, **55B**, (13), 8240–8248.

114. A. K. Przhevuskii and N. V. Nikonorov: *Opt. Mater.*, 2003, **21**, 729–741.

115. K. D. Oskam, R. T. Wegh, H. Donker, E. V. D. van Loef and A. Meijerink: *J. Alloys Compd*, 2000, **300–301**, 421–425.

116. Q. Y. Zhang and X. Y. Huang: *Prog. Mater. Sci.*, 2010, **55**, 353–427.

117. B. S. Richards: *Sol. Energy Mater. Sol. Cells*, 2006, **90**, 1189–1207.

118. K. Deutschbein, C. C. Pautrat and I. M. Svirchevsky: *Rev. Phys. Appl.*, 1967, **2**, 29.

119. V. Sudarsan, D. Jain, R. K. Vatsa and C. G. S. Pillai: *J. Lumin.*, 2010, **130**, 1379–1383.

120. Y. C. Yan, A. J. Faber, H. de Waal, P. G. Kik and A. Polman: *Appl. Phys. Lett.*, 1997, **71**, (20), 2922–2924.

121. R. Praveena, K. H. Jang, C. K. Jayasankar and H. J. Seo: *J. Alloys Compd*, 2010, **496**, 335–340.

122. D. A. Tran, G. H. Sigel, Jr and B. Bendow: *J. Lightwave Technol.*, 1984, **2**, (5), 566.

123. R. Allen, L. Esterowitz and I. Aggarwal: *IEEE J. Quantum Electron.*, 1993, **29**, (2), 303.

124. M. T. Murtagh, G. H. Sigel, Jr, J. C. Fajardo, B. C. Edwards and R. I. Epstein: *J. Non-Cryst. Solids*, 1999, **253**, 50–57.

125. S. Tanabe, K. Tamai, K. Hirao and N. Soga: *Phys. Rev. B*, 1996, **53B**, (13), 8358.

126. W. Seeber, E. A. Downing, L. Hesselink, M. M. Fejer and D. Ehrt: *J. Non-Cryst. Solids*, 1995, **189**, 218–226.

127. H. Ebendorff-Heidepriem, W. Seeber and D. Ehrt: *J. Non-Cryst. Solids*, 1995, **183**, 191–200.

128. G. Lakshminarayana, H. C. Yang and J. R. Qiu: *J. Solid State Chem.*, 2009, **182**, 669–676.

129. G. Lakshminarayana and J. R. Qiu: *J. Alloys Compd*, 2009, **481**, 582–589.

130. A. Konishi, R. Kanno and Y. Kawamoto: *J. Alloys Compd*, 1996, **232**, 53–59.

131. M. Ahrens, G. Scholz, M. Feist and E. Kemnitz: *Solid State Sci.*, 2006, **8**, 798–806.

132. P. Y. Jia, J. Lin and M. Yu: *J. Lumin.*, 2007, **122–123**, 134–136.

133. R. A. Hewes and J. R. Sarver: *Phys. Rev.*, 1969, **182**, 427.

134. H. J. Guggenheim and L. F. Johnson: *Appl. Phys. Lett.*, 1969, **15**, (2), 48–50.

135. L. F. Johnson and H. J. Guggenheim: *Appl. Phys. Lett.*, 1971, **19**, 44.

136. B. C. Collings and A. J. Silversmith: *J. Lumin.*, 1994, **62**, 271–279.

137. K. S. Lim: *Lasers Electron. Opt. Soc.*, 1999, **3**, 674–675.

138. N. J. Krasutsky: *J. Appl. Phys.*, 1983, **54**, 1261.

139. W. Lenth and R. M. Macfarlane: *J. Lumin.*, 1990, **45**, 346.

140. U. Oetliker, M. J. Riley, P. S. May and H. U. Giidel: *J. Lumin.*, 1992, **53**, 553.

141. H. Ni and S. C. Rand: *Opt. Lett.*, 1992, **17**, 1222.

142. R. M. Macfarlane, A. J. Silversmith, F. Tong and W. Lenth: in 'Laser materials and laser spectroscopy', (ed. Z. J. Wang and Z. M. Zhang), 24; 1989, Singapore, World Scientific.

143. S. Duffy, J. P. R. Wells, H. G. Gallagher and T. P. J. Han: *J. Cryst. Growth*, 1999, **203**, 405–411.

144. K. Ito, M. Yamagaa and N. Kodamab: *J. Alloys Compd*, 2006, **408–412**, 766–770.

145. A. H. Krumpel, E. van der Kolk, D. Zeelenberg, A. J. J. Bos, K. W. Krämer and P. Dorenbos: *J. Appl. Phys.*, 2008, **104**, (7), 073505.

146. A. Sarakovskis, J. Grube, A. Mishnev and M. Springis: 'Up-conversion processes in NaLaF$_4$:Er^{3+}', *Opt. Mater.*, 2009, **31**, (10), 1517–1524.

147. E. van der Kolk, P. Dorenbos, K. Krämer, D. Biner and H. U. Güdel: 'High-resolution luminescence spectroscopy study of down-conversion routes in NaGdF$_4$:Nd^{3+} and NaGdF^4:Tm^{3+} using synchrotron radiation', *Phys. Rev. B*, 2008, **77B**, 125110.

148. J. F. Suyver, J. Grimm, M. K. van Veen, D. Biner, K. W. Krämer and H. U. Güdel: *J. Lumin.*, 2006, **117**, 1, 1–12.

149. J. F. Suyver, J. Grimm, K. W. Krämer and H. U. Güdel: *J. Lumin.*, 2005, **114**, (1), 53–59.

150. P. R. Diamente, M. Raudsepp and F. C. J. M. van Veggel: *Adv. Funct. Mater.*, 2007, **17**, 363–368.

151. C. Li, J. Yang, P. Yang, H. Lian and J. Lin: *Chem. Mater.*, 2008, **20**, 4317–4326.

152. A. Bednarkiewicza, A. Mechb, M. Karbowiakb and W. Strek: *J. Lumin.*, 2005, **114**, 247–254.

153. W. Ryba-Romanowski, P. Solarz, G. Dominiak-Dzik and M. Gusowski: *Opt. Mater.*, 2006, **28**, 77–84.

154. V. K. Tikhomirov, D. Furniss, A. B. Seddon, I. M. Reaney, M. Beggiora, M. Ferrari, M. Montagna and R. Rolli: *Appl. Phys. Lett.*, 2002, **81**, (11), 1937–1939.

155. M. Beggiora, I. M. Reaney and M. S. Islam: *Appl. Phys. Lett.*, 2003, **83**, (3), 467–469.

156. S. Haas, A. Hoell, R. Wurth, C. Rüssel, P. Boesecke and U. Vainio: *Phys. Rev. B*, 2010, **81B**, (184), 207.

157. Y. Mita, Y. Wang and S. Shionoya: *Appl. Phys. Lett.*, 1993, **62**, 802.

158. P. A. Tick, N. F. Borrelli, L. K. Cornelius and M. A. Newhouse: *J. App. Phys.*, 1995, **78**, (11), 6367.

159. S. González-Pérez, F. Lahoz, J. M. Cáceres, V. Lavín, I. da Silva, J. González-Platas and I. R. Martín: *Opt. Mater.*, 2007, **29**, 1231–1235.

160. V. K. Tikhomirov, A. B. Seddon, M. Ferrari, M. Montagna, L. F. Santos and R. M. Almeida: *J. Non-Cryst. Solids*, 2004, **337**, 191–195.

161. M. Mattarelli, V. K. Tikhomirov, A. B. Seddon, M. Montagna, E. Moser, A. Chiasera, S. Chaussedent, G. Nunzi Conti, S. Pelli, G. C. Righini. L. Zampedri and M. Ferrari: *J. Non-Cryst. Solids*, 2004, **345–346**, 354–358.

162. B. Boulard, O. Péron, Y. Jestin, M. Ferrari and C. Duverger-Arfuso: *J. Lumin.*, 2009, **129**, 1637–1640.

163. M. Takahashi, M. Izuki, R. Kanno and Y. Kawamoto: *J. Appl. Phys.*, 1998, **83**, 3920.

164. L. L. Kukkonen, I. M. Reaney, D. Furniss and A. B. Seddon: *Phys. Chem. Glasses*, 2001, **42**, (3), 265–273.

165. G. Litscher, Z. Xie, L. Wang and I. Gaischek: *N. Am. J. Med. Sci.*, 2009, **1**, (5), 226–231.

166. G. Litscher, Z. Xie, L. Wang and I. Gaischek: *N. Am. J. Med. Sci.*, 2009, **1**, (5), 226–231.

167. F. Lahoz, I. R. Martín, J. Méndez-Ramos and P. Núñez: *J. Chem. Phys.*, 2004, **120**, (13), 6180.

168. J. L. Sommerdijk: *J. Lumin.*, 1973, **8**, 126–130.

169. J. Zhang, D. He, Z. Duan, L. Zhang, S. Dai and L. Hu: *Phys. Lett. A*, 2005, **337**, 480–486.

170. V. K. Tikhomirov, K. Driesen, C. Görller-Walrand and M. Mortier: *Opt. Express*, 2007, **15**, (15), 9535–9540.

171. S. F. León-Luis, J. Abreu-Afonso, J. Peña-Martínez, J. Méndez-Ramos, A. C. Yanes, J. del Castillo and V. D. Rodríguez: *J. Alloys Compd*, 2009, **479**, 557–560.

172. J. Méndez-Ramos, M. Abril, I. R. Martín, U. R. Rodríguez-Mendoza, V. Lavín and V. D. Rodríguez: *J. Appl. Phys.*, 2006, **99**, 113510.

173. V. D. Rodríguez, V. K. Tikhomirov, J. Méndez-Ramos, A. C. Yanes and V. V. Moshchalkov: *Sol. Energy Mater. Sol. Cells*, 2010, **94**, (10), 1612–1617.

174. G. A. Kumar, R. Riman, S. C. Chae, Y. N. Jang, I. K. Bae and H. S. Moon: *J. Appl. Phys.*, 2004, **95**, 3243.

175. L. Huang, T. Yamashita, R. Jose, Y. Arai and Y. Ohishi: *Glass Technol.*, 2008, **49**, (5), 225–228.

176. S. Ye, B. Zhu, J. Chen, J. Luo and J. R. Qiu: *Appl. Phys. Lett.*, 2008, **92**, 141112.

177. Z. Lin, X. Liang, Y. Ou, C. Fan, S. Yuan, H. Zeng and G. Chen: *J. Alloys Compd*, 2010, **496**, L33–L37.

178. D. Chen, Y. Wang, Y. Yu and E. Ma: *J. Solid State Chem.*, 2006, **179**, 1445–1452.

179. D. Chen, Y. Wang, Y. Yu, E. Ma, F. Bao, Z. Hu and Y. Cheng: *Mater. Chem. Phys.*, 2006, **95**, 264–269.
180. L. Zhou, D. Chen, W. Luo, Y. Wang, Y. Yu and F. Liu: *Mater. Lett.*, 2007, **61**, 3988–3990.
181. Y. Yu, Y. Wang, D. Chen and F. Liu: *Ceram. Int.*, 2008, **34**, 2143–2146.
182. X. Qiao, X. Fan and M. Wang: *Scr. Mater.*, 2006, **55**, 211–214.
183. S. A. Pollack and D. B. Chang: *J. Appl. Phys.*, 1988, **64**, 2885.
184. Y. Yu, D. Chen, Y. Wang, F. Liu and E. Ma: *J. Non-Cryst. Solids*, 2007, **353**, 405–409.
〔12〕 185. C. Li, S. Xu, R. Ye, S. Zhao, D. Deng and S. Zhuang: *Chin. Opt. Lett.*, 2010, **8**, 1.
186. J. R. Barros, C. Bocker and C. Rüssel: *Solid State Sci.*, 2010, **12**, 2086–2090.
187. D. Chen, Y. Wang, Y. Yu, E. Ma and L. Zhou: *J. Solid State Chem.*, 2006, **179**, 532–537.
188. Z. Duan, J. Zhang, W. Xiang, H. Sun and L. Hu: *Mater. Lett.*, 2007, **61**, 2200–2203.
189. F. Zeng, G. Ren, X. Qui and Q. Yang: *Physica B*, 2008, **403B**, 2471–2422.
190. G. Dantelle, M. Mortier, D. Vivien and G. Patriarche: *J. Mater. Res.*, 2005, **20**, (2), 472.
191. M. Mortier and G. Patriarche: *J. Mater. Sci.*, 2000, **35**, 4849.
192. D. Chen, Y. Wang, E. Ma, Y. Yu, F. Liu and R. Li: *J. Appl. Phys.*, 2007, **102**, (2), 023504.
193. D. Chen, Y. Wang, Y. Yu, F. Liu and P. Huang: *J. Rare Earths*, 2008, **26**, (3), 428.
194. D. Chen, Y. Wang, Y. Yu, P. Huang and F. Weng: *J. Solid State Chem.*, 2008, **181**, 2763–2767.
195. D. Chen, Y. Wang, Y. Yu, P. Huang and F. Weng: *Opt. Lett.*, 2008, **33**, (16), 1884–1886.
196. M. J. Dejneka: *J. Non-Cryst. Solids*, 1998, **239**, 149–155.
197. Z. Hu, Y. Wang, F. Bao and W. Luo: *J. Non-Cryst. Solids*, 2005, **351**, 722–728.
198. M. S. Chen: *J. Non-Cryst. Solids*, 1978, **27**, 257.
199. T. Ozawa: *Polymer*, 1971, **12**, 150.
200. D. Chen, Y. Wang, Y. Yu and E. Ma: *Mater. Chem. Phys.*, 2007, **101**, 464–469.
201. E. Ma, Z. Hu, Y. Wang and F. Bao: *J. Lumin.*, 2006, **118**, 131–138.
202. S. Ye, B. Zhu, J. Luo, J. Chen, G. Lakshminarayana and J. Qiu: *Opt. Express*, 2008, **16**, (12), 8989–8994.
203. S. González Pérez, I. R. Martín, F. Lahoz, D. Jaquec, P. Haro-González and N. Capuj: *J. Lumin.*, 2008, **128**, 905–907.
204. T. Honma, M. Kusatsugu and T. Komatsu: *Mater. Chem. Phys.* 2009, **113**, 124–129.
205. F. Liu, E. Ma, D. Chen, Y. Yu and Y. Wang: *J. Phys. Chem. B*, 2006, **110B**, (42), 20843–20846.
206. K. W. Krämer, D. Biner, G. Frei, H. U. Gudel, M. P. Hehlen and S. R. Lüthl: *Chem. Mater.*, 2004, **16**, 1244.
207. M. D. Mathews, B. R. Ambekar, A. K. Tyagi and J. J. Köhler: *J. Alloys Compd*, 2004, **377**, 162.
208. F. You, Y. Wang, J. Lina and Y. Tao: *J. Alloys Compd*, 2002, **343**, 151–155.
209. A. C. Yanes, A. Santana-Alonso, J. Méndez Ramos, J. del Castillo and V. D. Rodríguez: *J. Alloys Compd*, 2009, **480**, 706–710.
210. A. de Pablos-Martín, M. O. Ramírez, A. Durán, L. E. Bausá and M. J. Pascual: *Opt. Mater.*, 2010, **33**, 180–185.
211. S. Zhao, S. Xu, D. Deng, H. Wang, L. Huang and X. Fan: *Chem. Phys. Lett.*, 2010, **494**, 202–205.
212. S. Berneschi, S. Soria, G. C. Righini, G. Alombert-Goget, A. Chiappini, A. Chiasera, Y. Jestin, M. Ferrari, S. Guddala, E. Moser, S. N. B. Bhaktha, B. Boulard, C. Duverger Arfuso and S. Turrell: *Opt. Mater.*, 2010, **32**, 1644–1647.
213. S. Zhoua, H. F. Dong, G. F. Fenga, B. T. Wu, H. P. Zeng and J. R. Qiua: *Opt. Express*, 2007, **15**, (9), 5478.
214. N. A. Olsson: *J. Lightwave Technol.*, 1989, **LT-7**, 1071.
215. D. O. Caplan: *J. Opt. Fiber Commun. Rep.*, 2007, **4**, 225.
216. G. C. Righini, C. Arnaud, S. Berneschi, M. Bettinelli, M. Brenci, A. Chiasera, P. Feron, M. Ferrari, M. Montagna, G. Nunzi Conti, S. Pelli, H. Portales, C. Siligardi, A. Speghini and L. Zampedri: *Opt. Mater.*,2005, **27**, 1711–1717.
217. B. Jacquier, L. Bigot, S. Guy and A. M. Jurdyc: in 'Spectroscopic properties of rare earths in optical materials', Springer Series in Materials Science, Vol. 83, 430–461; 2005, Berlin, Springer.
218. R. V. Ramaswamy and R. Srivastava: *J. Lightwave Technol.*, 1988, **6**, (6), 984.
219. S. Honkanen, B. R. West, S. Yliniemi, P. Madasamy, M. Morrell, J. Auxier, A. Schülzgen, N. Peyghambarian, J. Carriere, J. Frantz, R. Kostuk, J. Castro and D. Geraghty: *Eur. J. Glass Sci. Technol. B*, 2006, **47B**, (2), 110–120.
220. J. L. Jackel: *Appl. Opt.*, 1988, **27**, 472.
221. A. Brandenburg: *J. Lightwave Technol.*, 1986, **LT-4**, 1580.
222. V. Tyagi and A. K. Varshneya: *J. Non-Cryst. Solids*, 1988, **238**, 186–192.
223. S. N. Houde-Walter and B. L. McIntyre: *J. Non-Cryst. Solids*, 1989, **107**, 316–322.
224. M. Dubiel, J. Haug, H. Kruth, H. Hofmeister and K. D. Schicke: *Mater. Sci. Eng. B*, 2008, **B149**, 146–151.
225. H. Portales, M. Mattarelli, M. Montagna, A. Chiasera, M. Ferrari, A. Martucci, P. Mazzoldi, S. Pelli and G. C. Righini: *J. Non-Cryst. Solids*, 2005, **351**, 1738–1742.
226. G. C. Righini, S. Pelli, M. Brenci, M. Ferrari, C. Duverger, M. Montagna and R. Dall'Igna: *J. Non-Cryst. Solids*, 2001, **284**, 223–229.
227. S. Berneschi, M. Bettinelli, M. Brenci, R. Dall'Igna, G. Nunzi Conti, S. Pelli, B. Profilo, S. Sebastiani, A. Speghini and G. C. Righini: *Opt. Mater.*, 2006, **28**, 1271–1275.
228. P. A. Tick: *Opt. Lett.*, 1998, **23**, (24), 1904–1905.
229. A. A. Lipovskii, D. V. Svistunov, D. K. Tagantsev, B. V. Tatarintsev and P. G. Kazansky: *Mater. Lett.*, 2004, **58**, 1231–1233.
230. D. K. Tagantsev, P. G. Kazansky, A. A. Lipovskii and K. D. Maluev: *J. Non-Cryst. Solids*, 2008, **354**, 1369–1372.
231. B. S. Richards: *Sol. Energy Mater. Sol. Cells*, 2006, **90**, 2329–2337.
232. B. S. Richards: *Sol. Energy Mater. Sol. Cells*, 2006, **90**, 1189–1207. 〔13〕

Authors Queries

Dear Author
During the preparation of your manuscript for publication, the questions listed below have arisen. Please attend to these matters and return this form with your proof. Many thanks for your assistance

Query Reference	Query	Remarks
1	Author: Reference cannot be cited in the abstract, please move it to the text.	
2	Author: Please confirm the running head.	
3	Author: Please confirm the change of equation is what you mean.	
4	Author: Please supply captions for Figs. 1–21	
5	Author: Please supply Fig. 2.	
6	Author: Please supply page no.	
7	Author: Please update info.	
8	Author: Please supply page no.	
9	Author: Please supply accessed date.	
10	Author: Please supply page no.	
11	Author: Please confirm whether the journal name is correct.	
12	Author: Please check whether page no. is correct.	
13	Author: Ref. 36 is the same as Ref. 41, Ref. 45 is the same as Ref. 47, Ref. 117 is the same as Ref. 232 and Ref. 165 is the same as Ref. 166, please check whether they are supplied correctly, please re-order the references according to citing sequence after all the references are confirmed and the same ones are removed.	

14	Fig3-21 are poor in quality and fig2 is missing, please supply a higher resolution version if possible.	